UNIVERSITÀ DEGLI STUDI DI PADOVA

DIPARTIMENTO DI INGEGNERIA INDUSTRIALE

CORSO DI LAUREA MAGISTRALE IN INGEGNERIA CHIMICA E DEI PROCESSI INDUSTRIALI

Tesi di Laurea Magistrale in

Ingegneria Chimica e dei Processi Industriali

Chitosan supported silver nanoparticles: an active and heterogenous catalyst for the reduction of organic dyes in waste water

Relatore:

Prof. Paolo Canu

Supervisore Istituto Ospitante:

Prof. Jyri-Pekka Mikkola

Laureanda:

CHIARA CONCETTA SICILIANO

ANNO ACCADEMICO 2021 - 2022

Abstract

The release of industrial effluent containing organic dyes in main streams of water is a big threat to the ecosystem as well as human beings. In this regards, several physical and chemical methods have been implemented for waste water purification before its discharge back to the natural resources. The aim of this thesis was the synthesis of a heterogenous catalysts containing silver nanoparticles loaded on glutaraldehyde cross-linked chitosan and its catalytic application for the reduction of organic dyes in its aqueous solution. Para-nitroaniline and phenol red are the two organic dyes that have been tested with the synthesized catalysts. The reduction of the dyes was carried out with sodium borohydride as a hydrogen source. FT-IR technique was used for the identification of different functional groups in cross-linked chitosan support and the catalyst. Besides that, the support and the catalyst have been characterized using other techniques, including powder XRD for determining the crystalline phase, SEM analysis for evaluating the sample surface, and ICP-OES for understanding how much silver is loaded onto the chitosan surface. The catalytic activity was tested by varying the catalyst amount, $NaBH_4$ amount, dye concentration, reaction temperature, and silver loading on the catalyst support. The progress of reaction was monitored by using UV-vis spectrophotometry. Kinetic studies of both organic reductions were carried out to identify a rate law, and compute the activation energy, pre-exponential factor using the Arrhenius equation, and partial reaction order. Aging of the catalyst was tested with both dyes, and the results demonstrated that after five recycling cycles, the catalyst was still active. In the case of phenol red dye, besides the reduction with the nanoparticles loaded chitosan and hydrogen source, an adsorption phenomenon on the catalyst surface was also identified. The studies demonstrated that the synthesized catalyst is highly active for the reduction of para-nitroaniline into para-phenylenediamine, and the reduction of phenol red dye.

Table of contents

Introduction

Water pollution for home and industrial use has always been an issue. The uncontrolled release of undesired compounds into waste water, particularly organic substances and organic dyes is a major cause of water contamination. Nowadays, more than 8000 organic dyes are manufactured in industries and part of them is then released in water, without a pre-treatment. The most problematic industries are those with high water use, like paper and textiles, because they are also the ones most responsible for leaking specific contaminants into water effluents. Consequently, a solution to this problem needs to be proposed, trying to handle in advance these substances to prevent their dispersion. Numerous strategies have been developed over the years to address this issue, including the employment of catalytic processes that would allow the decrease of organic chemicals or their conversion into less dangerous substances. The use of heterogeneous catalysis is one of the most modern and innovative methods for treating wastewater contaminated by organic dyes. The goal is to use a catalyst that is based on renewable, accessible, affordable, and safe materials.

The aim of this research is to contribute to the decrease and removal of organic dyes from water, focusing on the degradation of two compounds that are currently used as industrial dyes, such as p-nitroaniline and phenol red dye, with a catalytic reduction based on a heterogenous catalyst made of chitosan and silver nanoparticles and using $NaBH_4$ as hydrogen source. Additionally, the thesis aims to provide an understanding of the kinetics of the two reactions. The thesis is organized in four chapter:

- **Chapter 1**: Organic dye pollution.

  This chapter is a general overview about the problem of water pollution due to uncontrolled releases of organic dyes into the environment. The general characteristics of organic dyes, their effects on the environment and human beings and their classification are analysed here. Following that, the most common techniques for their degradation are assessed, with a stronger emphasis on heterogenous catalysis.

- **Chapter 2**: Material and experimental methods.

This chapter is dedicated to the description of the method and tools used for the monitoring of the reactions, the catalyst synthesis and catalyst characterization.

- **Chapter 3**: Catalyst characterization and catalytic activity.

  This chapter collects all the results of the experiments. It is divided into two sections: one contains the outcomes of the analyses characterizing the catalyst, particularly XRD, SEM, SEM-EDX, FT-IR and ICP-OES techniques, while the second part is dedicated to the results of the reactions of the two organic compounds. Reduction of p-nitroaniline and phenol red dye are carried out in different conditions, so the results are discussed evaluating the behaviour of the reacting systems with different concentration of catalyst, hydrogen source and reactants, and different temperatures. Finally, the catalyst is recycled and re-tested again.

- **Chapter 4**: Kinetic study.

  This chapter and the previous one represents the most significant section of the thesis. Kinetic study is carried out here, for both the catalytic reduction.

The thesis project was carried out partly at Chemistry Department of Umeå University, in the research group of professor Jyri-Pekka Mikkola. The experimental work was done with the supervision of Dr. Santosh Govind Khokarale. PhD student Mihn Van Din contributed to the catalyst characterization in the XRD, SEM and ICP-OES analysis. The last part of the work about the kinetic study and the writing of the thesis was carried out at University of Padua under the supervision of professor Paolo Canu.

Chapter 1
Organic dyes pollution

This chapter is an overview of the consequences related to the release of organic dyes in wastewater. The most used methods to deal with this problem are presented, followed by a summary about the goal of the thesis.

1.1 Applications of organic dyes and their impact on the environment

Organic dyes are one of the main classes of organic chemicals that represent an increasing environmental risk. Removal of these substances from the industrial effluents is a major issue since industries such as cosmetics, textiles, paper and food use various organic dyes in enormous amounts and usually discharge the wastewater without effective pre-treatment. Due to the large amounts of water required for dyeing operations, textile industry is one of the largest generators of polluted water effluents. During dyeing processes, 2-50% of the dye used in the industries is lost and discharged into wastewater. The first contamination in wastewater is color, which can be easily recognized since many dyes are visible in water at very low concentrations. Generally, dyes can be classified into natural dyes, which are extracted from vegetables, and synthetic dyes. The latter have aromatic structure, characterized by different functional groups and aromatic rings with delocalized electrons. Chromogene-chromophore is the acceptor of electrons, and its presence in the molecule is what gives the dye its color, and the presence of auxochrome groups, i.e. electron donors, is what gives the dye its dyeing capacity. Azo-group (-N=N-), methine group (-CH=), nitro group (-NO_2; -NO-OH) are example of functional groups which behave as chromophores. Carboxyl (-COOH), amino (-NH_2), sulphonate (SO_3H) and hydroxyl (-OH) groups are examples of auxochrome groups, which are ionizable moiety and determine the ability of the dye molecules to bind to the textile material. The withdrawal of coloured wastewater into the environment is a significant cause of eutrophication and non-aesthetic pollution, and it can lead to harmful consequences (Ali, 2010; Fernández *et al*., 2010; Akpan and Hameed, 2009; Saini, 2017). Organic dyes are toxic and harmful both for humans and animals and they are considered as a pollutant for water bodies and aquatic life. Large

quantities of these organic dyes and their derivatives are disposed in water reservoirs and soil, disrupting the biological activity of aquatic life and the photosynthesis process of plants, perhaps causing irreversible and unwanted ecological changes. They reduce light penetration and the amount of dissolved oxygen in water, influencing both aquatic fauna and flora. The non-biodegradability of these dyes, which causes them to accumulate in sediments, contributes to their polluting effects (Ali, 2010; Saini, 2017). Their poisonous impacts on ecosystems are of grave concern since some of these chemicals are partly thought to be endocrine disruptors (EDCs) and particularly, azo dyes are reported to be carcinogenic and mutagenic because their decomposition is presumed to be responsible for cancer in humans and animals (Akpan and Hameed, 2009; Saini, 2017). In recent years, many studies have been carried out concerning the removal of these dyes from industrial wastewater but, in some cases, their complete degradation is not possible. Since the aromatic structure in organic dyes is very complex, only few techniques can be considered efficient. Even if the number of organic dyes in wastewater is very low and usually they are visible considering their colourful nature, their resistance to light, heat, oxidation and reduction agents is a bottleneck in the effective degradation process (Mittal *et al*., 2009). With the constantly expanding manufacturing activities, there is the need to come up with an economical and efficient way to manage the dye contaminated wastewater (Ali, 2010).

1.2 Overview on different methods for the removal of organic dyes from wastewater effluents

The chemical variety of textile effluents makes it challenging to treat them using standard purification techniques and some treatments, like chlorination, are inadequate because they cause even less toxic dyes to emit mutagenic by-products (Saini, 2017). Researchers worldwide are working to identify practical and effective ways to remove colors from industrial effluents using either physical, chemical, or a combination of these techniques. Adsorption techniques and catalytic processes based on reduction, oxidation, photocatalytic degradation are the most used, efficient and selective ways to purify contaminated water since these processes can be carried out under mild reaction conditions as well as with easily available materials (Mittal *et al.*; 2009, Anbu Anjugam Vandarkuzhali *et al*., 2020; Wahab and Hussain, 2016; Asiri *et al*., 2011; Naseem *et al*., 2018). Nowadays, methods that are widely studied and therefore used are

adsorption, oxidation and biological treatments (Fernández *et al*., 2010; Saini, 2017).

1.2.1 Adsorption

Due to its affordability and effectiveness in removing colors from wastewater, adsorption is identified as one of the most valid and widely used techniques for the treatment of industrial water effluents. Adsorption is a rapid process and generates high quality products. The procedure involves the use of an adsorbent material characterized by large porosity, that is able to interact with the soluble dye and transfer it from the solution to the surface of the solid adsorbent. Different factors can influence the adsorption mechanism, such as temperature, pH, dye/adsorbent interaction and contact time, particle size and surface area of the solid adsorbent. At some point, the adsorbent reaches the saturation condition, namely, it is not able to remove organic dye anymore, therefore it must be recycled or burned and replaced with a new one (Anjaneyulu *et al*., 2005; Saini, 2017). The most commonly used adsorbent is activated carbon, but it is characterized by very high initial cost and problems connected to its recycling (Anjaneyulu *et al*., 2005). For this reason, alternatives have been studied, and among all the others, low-cost adsorbents from waste materials have been evaluated, such as bottom ash and deoiled soy. They have been studied for the removal of organic dyes and have been shown to be better for dye adsorption, less expensive and more easily accessible than commercially available materials (Mittal *et al*., 2009). Other alternatives to activated carbon are agricultural residues, such as wheat straw and corn-cob shreds, activated petroleum coke, chitosan (Anjaneyulu *et al*., 2005; Ma *et al*., 2019).

1.2.2 Oxidation

Due to its ease of management, oxidation is the chemical decolorization procedure most frequently utilized. It is a chemical reaction that involves the use of oxidizing agents like chlorine, ozone, Fenton reagents, oxygen/air and it causes the dye molecules aromatic rings to cleave (Anjaneyulu *et al*., 2005; Saini, 2017). Advanced oxidation processes (AOPs) are green techniques since solid secondary pollution is not generated and dyes completely degrade to CO_2, H_2O and low-molecular-weight molecules, such as aldehydes and inorganic compounds (Fernández *et al*., 2010).

Oxidation with hydrogen peroxide can be carried out in two different ways: homogeneous

systems and heterogenous systems. In the first case, oxidation is achieved thanks to soluble catalysts like Fenton reagents, or visible and ultraviolet light; in the second case, heterogenous agents are used, such as zeolites. Hydrogen peroxide oxidation helps decrease the color and toxicity of water effluent and can be useful for removing insoluble and soluble dyes. The primary benefit of using hydrogen peroxide is that it can be seen as a friendly oxidant because, during its breakage, water and oxygen are produced (Saini, 2017; Zaharia *et al*., 2009).

Ozone is a vigorous oxidizing agent, and its high oxidation potential allows it to efficiently degrade the conjugated double bonds of dye chromophores and other functional groups, like the aromatic rings of dyes. Therefore, an oxidation process by ozonation can be used for the decolorization of wastewater. It has a lot of advantages because ozone use is less dangerous than other oxidation processes since it does not require the storage of hazardous substances, as in the case of hydrogen peroxide-based oxidation or when other hazardous substances are used. Furthermore, ozonation can decrease organic matter and it is simple to convert residual ozone to oxygen (Tehrani-Bagha *et al*., 2010).

When H_2O_2 is present, the UV treatment of wastewater containing dyes can break down the dye into smaller organic molecules or even into final products like CO_2 and other inorganic oxides (Saini, 2017). For this reason, homogeneous UV-H_2O_2 oxidation has been discovered to be a particularly favored process for the removal of dye in water effluents. This method leads to the degradation and decolorization of organic dyes thanks to the simultaneous action of UV radiation and the presence of hydrogen peroxide. UV-H_2O_2 oxidation can be carried with solar radiation, and even though UV source is more efficient than sunlight and the effort connected to the construction of reactors that are able to use solar light is high, the photodegradation process is still good (Fernández *et al*., 2010).

1.2.3 Biological methods

The procedure of biological treatment is straightforward, affordable, and environmentally friendly, among other benefits. Fungi, algae and bacteria are examples of microorganisms that can be used for the removal of organic dyes from industry water effluents (Varjani *et al*., 2020). Usually, dyes are not influenced by different microorganisms under aerobic biological conditions in standard wastewater treatment and disposal facilities. On the other hand, they degrade in anaerobic conditions, resulting in the formation of aromatic amines that need to be

further degraded in an aerobic way. A consequence of this is that dyes typically resist aerobic bacterial biodegradation or, due to the toxicity of the dye, some microorganisms cannot be used on most of wastewater treatment. Therefore, to improve the process efficiency of degradation, genetically modified organisms can be used. Under fully aerobic circumstances, only bacteria with specialized azo dye reduction enzymes were discovered to destroy dyes. Therefore, the complete degradation of organic dyes can be achieved in an anaerobic environment and can be distinguished into two steps: first, the dye is degraded completely and give rise to the formation of harmful aromatic amines that need to be converted in the second step, during which there is a switch from anaerobic to aerobic conditions (Sriram *et al*., 2013; Varjani *et al*., 2020). The use of living microorganisms entails mild conditions, namely drastic pH and temperature cannot be used. The positive aspect of these methods is that they can inexpensively remove colors from huge volumes of wastewater (Fernández *et al*., 2010).

1.3 Disposal of organic dyes through catalysis

Organic dye effluent is one of the most challenging industrial wastewaters to clean and even if many technologies have been developed, catalysis is an essential way to purify water from organic pollutants. It has received a lot of interest from scientific groups since this technique can convert organic molecules into inorganic compounds. Thus, effective catalysis must be developed for the treatment of dye wastewater. Catalyst features, such as the structure and distribution of active sites, are fundamental for reaction efficiency, therefore it is important to adjust the composition, shape, and size of the catalyst. In the last decades, a lot of studies have been carried out on wastewater treatment through the use of photocatalysts or biocatalysts (He *et al*., 2018).

1.3.1 Nanoparticles based catalysts

With applications in numerous research and development domains, such as biology, chemistry, material science, medicine, and physics, nanotechnology is a developing and advanced technology. Nanoscale materials in general have drawn a lot of attention since the advent of nanoscience and nanotechnology (Khataee and Kasiri, 2009). Nanoparticles contain higher fraction of atoms at the edges and the corners than the bulk material; it is reasonable to assume that the exposed atoms at the corners and edges are chemically more reactive than the ones in

the center. According to different studies, nanomaterials are employed in a number of catalytic processes, such as hydrogenation, oxidation, reduction, coupling, and several other processes (Islam *et al*., 2018).

One of the most recent technologies appears to be heterogenous photocatalysis employing TiO_2 nanoparticles as the photocatalyst (Khataee and Kasiri, 2010). The main advantage of this process is its destructive nature, without generating secondary toxic materials (Asiri *et al*., 2011). Moreover, it does not include mass transfer, can be performed in ambient environment, such that atmospheric oxygen is used as an oxidant, and may result in the complete mineralization of organic carbon. TiO_2 nanoparticles are widely accessible, affordable and non-toxic, and photocatalytic process involving these substances is gaining popularity due to its inexpensive cost, when sunlight is used (Khataee and Kasiri, 2010). The decomposition of different types of organic pollutants can be performed and the method is characterized by a degradation of the complex organic structure into CO_2, H_2O and inorganic acids following a photocatalytic degradation (Asiri *et al*., 2011). The combination of $UV/TiO_2/O_2/H_2O_2$ is a good strategy for a photocatalytic oxidation of dyes in aqueous solutions for the degradation of the organic compound and achieved in transforming the reactant into CO_2, H_2O, NO_3^-, PO_4^{3-}, and halide ions (Wahab et al., 2016). Heterogenous photocatalysis can be carried out also with metal chalcogenides like CuS, ZnS and CdS, thanks to their capacity to absorb solar energy, particularly in the visible spectrum. Reduced graphene oxide (rGO) can be used with chalcogenide semiconductor materials, since a support to increase the surface area is needed. CuS/rGO nanocomposites have good photocatalytic performance for the elimination of organic dyes (El-Hout *et al*., 2020).

On the other hand, catalysis can be used for chemical reduction, employing reducing agents like sodium borohydride, thiourea dioxide and sodium hydrosulfide, to achieve an effective decolorization of many dyes (MeenaKumari and Philip, 2015). Compared to other methods, catalytic reduction is preferred, since in the treatment of some dyes, such as Congo red, the reduction products find uses in a wide range of sectors. While other processes have a variety of disadvantages, such as high costs, the transfer of dye only from one medium to another, slow processing, and the production of toxic byproducts, catalytic reduction involves the cleavage of molecules, which results in the production of less toxic and environmentally friendly products. (Naseem *et al*., 2018). In this regard, supported nanometal catalysts comprised of metals such as silver, palladium, gold and platinum stabilized on various heterogenous supports such as

carbonaceous materials, metal oxide or polymeric supports are widely used for the degradation of organic dyes in aqueous medium (Islam *et al.*, 2018; Malik and Nath, 2020). Metal nanoparticles on the support are generally produced through in situ reduction of metal ions coming from the metal salts added to the support dispersion (Naseem *et al*., 2018). Chemical reduction can degrade dye in a way that is thermodynamically favored, but not kinetically. Gold and silver nanoparticles are particularly interesting in different organic reactions. They lower the kinetic barrier and, consequently, the activation energy, making the reactions both thermodynamically and kinetically possible (MeenaKumari and Philip, 2015). In particular, supported nanometal catalysts based on silver metal are thought to be a primary choice for the processing of organic dyes in water since the precursors needed to make the catalysts are considerably less expensive and more widely accessible than other precious metals. Silver nanoparticles (AgNPs) have catalytic efficacy that depends on their size and shape, and they typically have high reactivity and selectivity. AgNPs catalytic activity rises as their size decrease because of their improved surface to volume ratio. Agglomeration, which significantly lowers their catalytic efficiencies, becomes a critical issue due to the increase in surface energy of AgNPs. Several inorganic and organic matrices have been employed as support for the immobilization of silver nanoparticles to deal with this problem. Heterogeneous supports such as mesoporous carbon, graphene oxide, mesoporous silica, cotton fabric, metal oxides can be employed for the synthesis of silver-based catalysts. It has been shown that catalytic reduction using a catalyst based on silver nanoparticles is an effective method for properly disposing of organic dyes such methyl orange, methylene blue, methyl orange, Congo red, 4-nitroaniline (Malik and Nath, 2020; Islam *et al*., 2018).

1.3.2 Chitosan based catalysts

Chitosan is a biopolymer, and it can be defined as the N-deacetylated derivative of chitin. It is a linear and semi-crystalline polysaccharide containing copolymers of D-glucosamine (deacetylated units) and N-acetyl-D-glucosamine (acetylated units) linked by beta (1,4) glycosidic bonds. It is obtained from the partial deacetylation of the chitin, through alkaline or enzymatic methods and the goal is to eliminate acetyl groups ($COCH_3$), although the process is virtually never completely effective. It is possible also to classify the chitosan according to the degree of deacetylation, which is generally defined as glucosamine/N-acetyl glucosamine ratio.

Depending on this value, the distinction between chitosan and chitin can be defined: when the percentage of N-acetyl glucosamine is higher than glucosamine, the biopolymer is known as chitin, and when the percentage of glucosamine exceeds N-acetyl glucosamine the compound is called chitosan. After cellulose, chitin is the most abundant biopolymer on earth. Chitin and cellulose have a similar structure, but chitin has an acetamide group ($NHCOCH_3$) in C-2, where cellulose has hydroxyl group instead. Chitosan is characterized by same configuration, where amino group are placed in C-2 position (Figure 1.1) (Hamed *et al*. 2016).

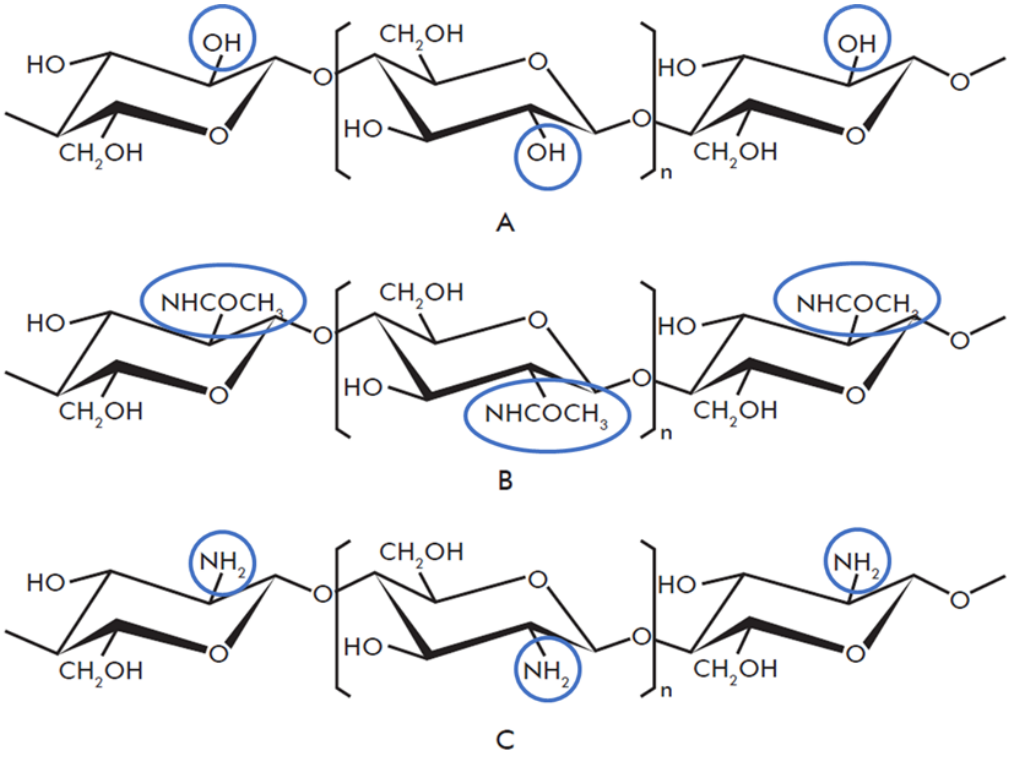

Figure 1.1 - Chemical structure of A) cellulose, B) fully acetylated chitin and C) fully deacetylated chitosan (Ramírez et al., 2010)

Different sources can be used to produce chitin and chitosan, such as arthropods, mollusks, fungi, algae, but the more innovative way is the use of crustacean shell, like crabs and shrimps, due to the availability of wastes from seafood processing industry. Shellfish processing companies produce large amount of waste annually, which is typically burned, landfilled or thrown in the sea. Hence, the removal of chitin from crustacean shells and utilization of it either in its natural state or after further processing may be a way of minimizing waste and produce valuable chemicals with excellent biological qualities. Since crustacean processing waste has a negative impact on the environment, it is considered as the preferred choice for chitin/chitosan

extraction due to its abundance and chitin content. Chitin and chitosan are widely used in many fields, like in food industry, especially for the packaging of food thanks to their preservative capacity, and also for their antioxidant activity. Moreover, they are used in pharmaceutical and biomedical industry, in agriculture, as chemical pesticides and for soil treatment, in paper industry and in textiles, to produce non-allergenic fibers (Ramírez *et al*., 2010; Hamed *et al*. 2016). The main problem of chitin is its insolubility in water and most of organic solvents; therefore, chitosan is preferred for many applications. In general, because it contains amine groups, chitosan is a weak base (pKa = 6.3) and is highly soluble in acidic solutions (mostly below pH = 6.0). Because of the protonation of the amine groups at low pH levels, chitosan can act as a water-soluble cationic polyelectrolyte. However, at pH > 6, the biopolymer loses its charge and becomes insoluble, since the amine groups of chitosan residues are deprotonated (Figure 1.2) (Jiménez-Gómez and Cecilia, 2020).

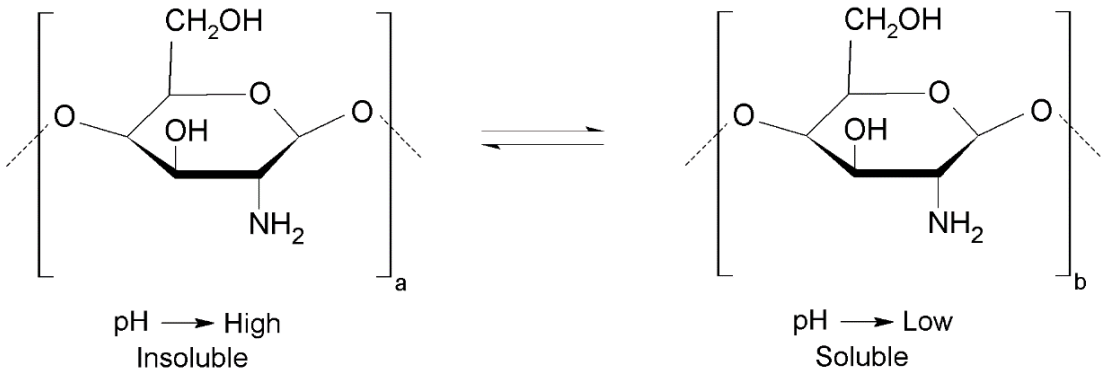

Figure 1.2 - Chemical structure of chitosan as a function of pH. Insoluble (pH>6) and soluble (pH<6) (Jiménez-Gómez and Cecilia, 2020)

For this reason, chitosan is usually treated in acidic aqueous solution to create products such as nanofibers, coatings, hydrogels, and films. Thanks to the complex molecular structure of chitosan characterized by different functional groups, like amino and hydroxyl fraction, chitosan has been used in catalysis. Particularly, the presence of amino, primary hydroxyl and secondary hydroxyl functional groups is useful for the generation of covalent and non-covalent modifications, such that chitosan can be used as a substrate in metal loaded heterogeneous catalyst for the reduction of the toxic organic pollutants. In this way it is possible to substitute other synthetic polymers with chitosan, obtaining very good results and using a renewable source (Hamzavi *et al*., 2019; Khan *et al*., 2020).

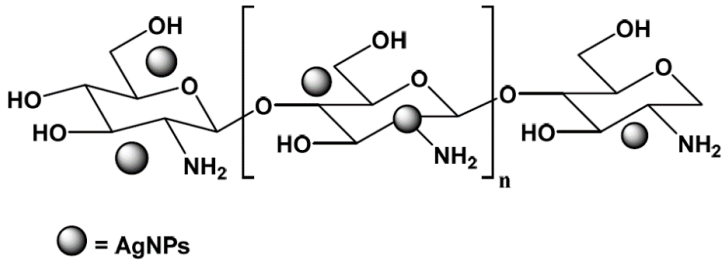

Figure 1.3 - Chemical structure of silver nanoparticles on chitosan (Hamzavi et al., 2019)

The use of silver nanoparticles on chitosan in catalytic reduction procedures for the processing of impure water containing organic dyes has been successfully investigated. In this regard, the contributions of Sargin (2019) and Zheng and Wang (2012) have a fundamental role. In these investigations, hydrogel chitosan is used as substrate to synthetize the catalyst (Figure 1.3). In both cases, chitosan has been treated with crosslinker agents, which are glutaraldehyde and N,N′-methylene bis-acrylamide (MBA), respectively. In Sargin's work (2019) the preparation of the support is carried out by dissolving chitosan in acetic acid solution, such that a viscous medium is created. In order to get a final substrate in spherical shape, chitosan acid solution is dropped into alkaline medium. Then, chitosan beads become stable and can be washed and collected by filtration, until a neutral pH is reached. However, chitosan beads shrink and lose their spherical shape after drying. Furthermore, since the amine groups are protonated in an acidic medium, dried chitosan can dissolve in acidic solution if it is not covalently crosslinked, and this means that its further use is reduced. This is the reason why crosslinking agents are used: in this way, a hydrogel is obtained, thanks to electrostatic interactions of amino and hydroxyl groups. The structure is stabilized, and chitosan beads become insoluble at low pH (Figure 1.4).

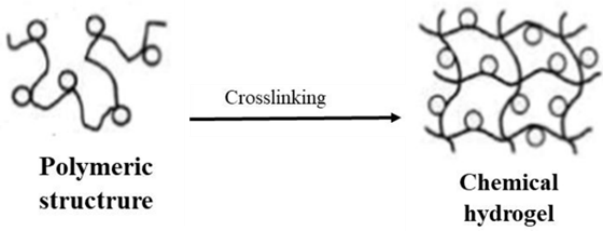

Figure 1.4 - Chitosan hydrogel obtained with crosslinking interactions. Adapted from Jiménez-Gómez and Cecilia, 2020

Glutaraldehyde is one of the most used crosslinkers for chitosan, since it is a dialdehyde that exhibits reactivity to the amino functionalities of the biopolymer. In order to produce stable

imine bonds (-C=NH-), the carbonyl groups at the two ends of the glutaraldehyde molecule react with the -NH_2 functionalities of the polymeric chains of chitosan (Jiménez-Gómez and Cecilia, 2020; Sargin, 2019).

1.4 Aim of the thesis

Studies on the manufacturing of silver nanoparticles supported on chitosan catalysts are a few, but promising. In literature, there are some studies about the use of Ag/chitosan catalysts for the reduction of nitroaromatic compounds, such as 2-nitrophenol and 2-paranitroaniline, and organic dyes, such as methylene blue, Congo red, methyl orange (Sargin, 2019; Khan *et al*., 2020; Zheng and Wang, 2012; Kaloti and Kumar, 2018). Therefore, the activity of Ag nanoparticles loaded on chitosan support in the degradation of organic dyes should be further explored.

The present work reports the catalytic reduction of para-nitroaniline and phenol red dye with chitosan supported silver nanoparticles as catalyst (Ag/CH). p-Nitroaniline (PNA) (Figure 1.5) is an aromatic compound and can be released in the environment from different sources, since it is a crucial substance to produce pesticides, pharmaceuticals and dyes.

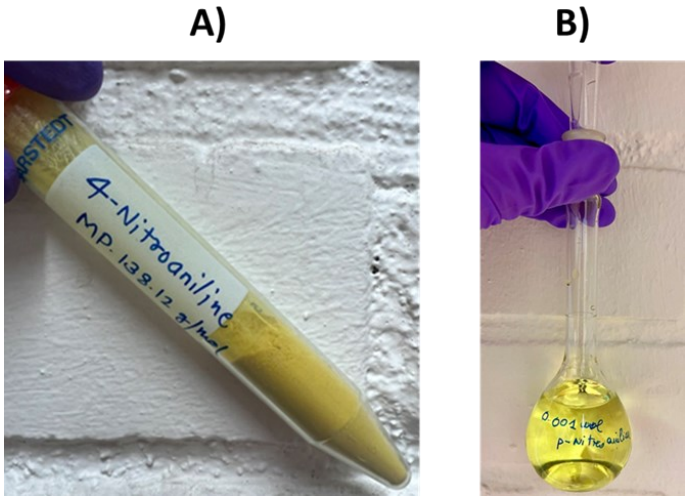

Figure 1.5 - A) p-nitroaniline in powder form; B) 0.001 M aqueous solution of p-nitroaniline

The presence of a nitro group in the aromatic ring (Figure 1.6A) enhances the stability to resist chemical degradation and it can cause ecological damage if released as contaminant, since it dissolves in water. Many nations have identified PNA as a priority contaminant due to its toxicity and carcinogenic effects. Therefore, reduction of PNA is industrially and

environmentally important (Sun *et al*., 2007). Chemical degradation with silver nanoparticles and Ag/CH as catalyst have been already studied for the reduction of p-nitroaniline (Edison *et al*., 2016; Sargin, 2019).

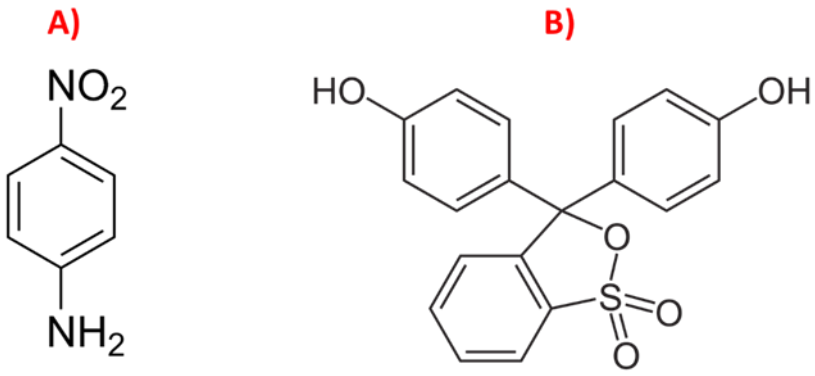

Figure 1.6 - Chemical structure of A) p-nitroaniline and B) phenol red dye

Phenol red dye (PRD) (Figure 1.6B) is a water-soluble substance belonging to organic dyes. It can be used in many different types of applications such as a pH indicator in cell cultures and in home swimming pool tests, diagnostic aid for determination of renal function or estrogenic properties (https://pubchem.ncbi.nlm.nih.gov/compound/Phenol-red; Tan *et al*., 2011). It has been shown that PRD has a mutagenic effect and causes serious eye damage as well as skin and respiratory irritation (Chung *et al*., 1981; https://pubchem.ncbi.nlm.nih.gov/compound/Phenol-red; https://terpconnect.umd.edu/~choi/MSDS/Sigma-Aldrich/PHENOL%20RED.pdf). The reduction of PRD with an heterogenous catalyst has not been studied thoroughly; indeed, only few research projects in this field are available in the literature. Fine copper nanoparticles on amine functionalized SBA-15 are used in the catalytic reduction process upon treatment of phenol red dye, malachite green and bromophenol blue. After 5 minutes of reaction time, mesoporous Cu/NH_2-SBA-15 demonstrated good reduction performance of triphenyl methane dyes, such as malachite green, bromophenol blue and phenol red, with $NaBH_4$ to their respective leuco forms (Anbu Anjugam Vandarkuzhali *et al*., 2020). On the other hand, no papers were found about the use of chitosan supported silver nanoparticles as catalyst.

This project is focused on the study of the Ag/CH catalyst reduction of PNA and PRD in its aqueous solution with $NaBH_4$ as a hydrogen source. Initially, glutaraldehyde crosslinked chitosan was synthesized and used as a carrier to produce Ag/CH catalyst. The materials prepared from this process were then evaluated using different analysis techniques. The two

organic compounds were reduced using chitosan-based materials, with various reaction conditions. The reusability of the Ag/CH was checked, and catalysts with different Ag loading on cross-linking chitosan were prepared and tested in the reductions.

Chapter 2
Material and experimental methods

This chapter is dedicated to the presentation of instrumental tools, experimental procedures and analysis methods used for the thesis project. The experiments were carried out in the Technical Chemistry labs in Umeå University.

2.1 UV-vis spectroscopy

UV-vis spectrophotometry is a commonly analytical technique that involves measuring the absorption of light in the ultraviolet (UV) and visible (vis) regions of the electromagnetic spectrum by a sample. A beam of light passes through the sample, which absorbs part of it and the remaining one is transmitted. Transmittance, reflectance, and photoluminescence (fluorescence and phosphorescence) modes are frequently used for UV-Vis measurements. Measurements of transmittance and reflectance must be made in comparison to a reference material, whereas photoluminescence acquisitions can be viewed as absolute measures. The UV-vis spectrophotometer consists of four main components: polychromatic light source, a sample holder, a detector for the measurement of the radiation that interact with the sample and wavelength selectors to separate the radiations into various components. The light source produces a beam of light that is directed towards the sample, while the detector measures the intensity of the light that is transmitted through the sample. The sample is usually dissolved in a solvent and placed in a cuvette, which is a small container made of quartz or glass that has two parallel sides. The cuvette is placed in the sample holder, where it is hit by a beam of light. The amount of light absorbed by the sample is determined by measuring the difference in the intensity of the light before and after it passes through the material. This difference is called the absorbance (A) and is defined according to Beer-Lambert's law ($A = \varepsilon cl$) in which A is proportional to the molar absorptivity ε, the concentration of the species in the sample c, and the path length of the light through the sample l (Picollo *et al*., 2018). The UV-vis spectrophotometer is useful for determining the concentration of an analyte in a sample,

identifying the presence of certain functional groups in molecules, and monitoring chemical reactions. In this work, UV-spectra to evaluate the progress of reactions were obtained using a UV-3100PC Spectrophotometer (VMR International BV, Geldenaaksebaan, Leuven, Belgium).

2.1.1 Progress of reaction with UV-vis spectrophotometer

UV-visible spectroscopic studies were done to evaluate the progress of the reduction of reactants. This technique can be used to detect PNA and PRD because they are UV sensible. Before performing the sample analysis, the UV-vis spectrophotometer must first be calibrated. A quartz cuvette was filled with distillate water and the blank calibration was started. Then, the samples were diluted with distillate water and put into the same cuvette, which was loaded in the internal sample holder. UV light hit the sample and measured the absorbance values in the range of 200-600 nm for the PNA and 200-800 nm for the PRD. In the case of 0.001 M PNA aqueous solution, 0.1 ml of reacting solution was collected and diluted with 1 ml of distillate water; for PRD, 0.05 ml of reacting solution were diluted with 1 ml of distillate water. The measurements were done each 3 minutes, such that different curves of absorbance vs wavelength were obtained at different time intervals. According to literature, the characteristic adsorption peak of PNA and PRD are λ_{max} = 380 nm and λ_{max} = 440 nm, respectively (Sun *et al*., 2007; Tan *et al*., 2011). As the reductions proceeded, the graphs obtained at different time intervals allowed to monitor the progress of the reactions, thanks to the decrease in intensity of the characteristic peaks of the reactants until they disappeared completely. To quantify the progress of reaction and determine the conversion, a calibration was required.

2.1.2 Calibration with UV-vis spectrophotometer

Calibration is the procedure used to get the concentration of PNA during reactions, starting from its absorbance value measured with the UV-spectrophotometer. Four different samples (Table 2.1) with different concentrations of PNA were prepared (actual concentration) and analyzed through the spectrophotometer to get the curves of absorbance vs wavelength (Figure 2.1A). Since each solution had a specific concentration, four points of (absorbance, concentration) were obtained considering the peak at λ = 380 nm. These were fitted and the corresponding equation linking absorbance (Y-axis) and concentration (X-axis) in the form y =

mx was obtained. The fitting was done with Excel, imposing the intercept (0,0) and the resulting curve is shown in Figure 2.1B.

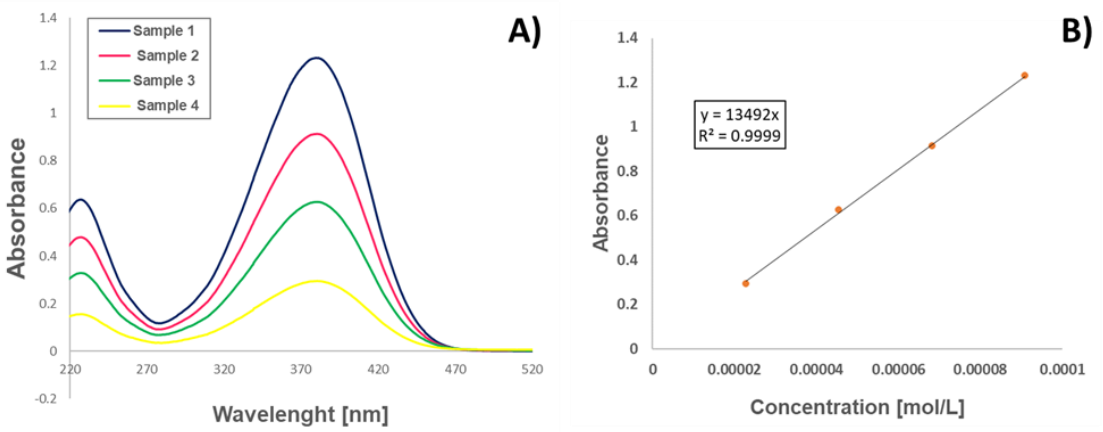

Figure 2.1 - A) UV spectra of the four samples used for calibration; B) Calibration curve

The measurements with UV machine were done with diluted sample, since the cuvette was filled with 0.1 mL of PNA mixed with 1 mL of distillate water. Therefore, concentration in the calibration curve was a diluted one (Table 2.1). A dilution factor was needed, defined as the ratio between the total volume analyzed in the UV spectrophotometer (1.1 mL) and the volume taken from the PNA solution (0.1 mL):

$$DF = \frac{total\ volume}{sample\ volume} \tag{2.1}$$

Actual concentration and the diluted concentration are linked one to each other through DF: $c_{actual} = c_{diluted}\, DF$. Therefore, when a reacting sample was tested with UV-spectrophotometer, the concentration at that time c(t) was computed from the absorbance value, that is converted into diluted concentration through the calibration equation; then, actual concentration was calculated through DF. Percentage of conversion during reaction can be computed with Equation 2.2.

$$\%\ Conversion = \frac{c(t=0) - c(t)}{c(t=0)} \cdot 100 \tag{2.2}$$

For PRD, no calibration was computed; conversion was evaluated directly from absorbance values (Equation 2.3).

$$\%\, Conversion = \frac{A(t=0) - A(t)}{A(t=0)} \cdot 100 \qquad (2.3)$$

Table 2.1 *- Actual concentration and diluted concentration during calibration for p-nitroaniline solution*

	Actual concentration [M]	**Diluted concentration [M]**
Sample 1	0.001	0.000091
Sample 2	0.000751	0.0000685
Sample 3	0.000501	0.0000455
Sample 4	0.00025	0.0000227

2.2 Characterization techniques

2.2.1 X-Ray powder Diffraction (XRD)

X-ray powder diffraction is a very common technique, useful to determine the atomic and molecular structure of materials. It can analyze crystalline materials and give information about the composition, the phase and unit cell dimensions. The method is based on irradiating the sample with incident X-rays and then measuring the intensities and scattering angles. X-rays are electromagnetic waves with a specific wavelengths, or beams of photons with associated energies. Other electromagnetic waves include visible light, radio waves and γ-rays. X-ray light waves irradiate the crystal and propagate through it, encountering lattice points from which they diffract. Bragg's law summarizes this procedure through an equation: $n\lambda=2d_{hkl}sin\theta$. The parameters included in this expression are the wavelength λ of the X-rays used, the spacing between a particular set of planes d_{hkl}, with hkl that are the miller indices, the diffraction angle θ and n, that is an integer, and represents the order of interference (Figure 2.2) (Ermrich and Opper, 2013). The sample placed inside the diffractometer is rotated with respect to the X-ray source, with an angle equal to θ. The diffracted X-rays can be detected thanks to X-rays detector, and then processed and counted. The detector rotates at twice the rate of the sample, so its angle is equal to 2θ. In this way, based on the 2θ angles, diffraction peaks are computed,

which can be converted into d-spacings. Through the calculation of the d-spacings of multiple peaks, the identification of the compound can be carried out and the crystal structure parameters of the sample can be obtained. Usually, it is necessary to use some database, to do a comparison between the obtained d-spacings with the standard one.

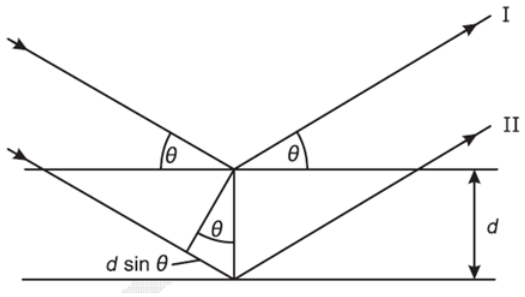

Figure 2.2 - Graphical representation of Bragg's law (Ermrich & Opper, 2013)

In this work, data were collected using a PANalytical X'Pert3 Powder Diffractometer (Figure 2.3) equipped in a 2θ range between 7° and 60° at room temperature with a scan rate of 1°/min using Cu Kα radiation.

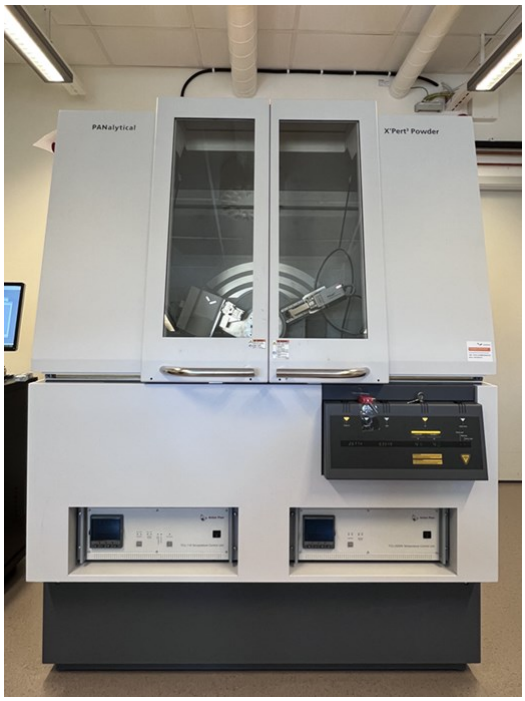

Figure 2.3 - PANalytical X'Pert3 Powder Diffractometer used for the catalyst characterization

2.2.2 Scanning Electron Microscopy (SEM)

Scanning electron microscopy (SEM) is an analytical technique that uses a beam of electrons to image the surface of a sample and can be used to study the morphology of various materials. The technique is based on the interaction between the sample and a focused beam of electrons that is scanned across the surface of the sample. An electron source, a set of electromagnetic lenses, and a detector are some of the elements that constitute the SEM. The electron source produces a beam of electrons, which is accelerated by an electric field toward the sample. While some electrons in the sample are scattered or absorbed by the atoms, others penetrate the sample and interact with the deeper layers. A detector collects the secondary and scattered electrons that result from the interactions, and the signal is then used to create an image of the surface of the sample. Usually shown on a computer screen, the image can be digitally modified and altered to conduct a deeper examination. SEM can also be used for energy dispersive X-ray spectroscopy (EDS), which enables the identification of the elements in the sample, and electron backscatter diffraction (EBSD), which may be employed to analyze the crystal structure and the orientation of the material. The morphology of the catalysts in this project was analysed using a Zeiss Merlin FEG-SEM instrument (Oberkochen, BW, Germany) equipped with an in-lens secondary electron detector.

2.2.3 Inductively Coupled Plasma – Optical Emission Spectroscopy (ICP-OES)

Inductively coupled plasma optical emission spectroscopy (ICP-OES) is an analytical technique used to identify the qualitative and quantitative elementary composition in samples. ICP-OES system is characterized by a sample introduction system, an argon gas plasma source, a spectrophotometer, and a detector. Typically, a solvent is used to dissolve the sample before it is sprayed into the plasma using a nebulizer or spray chamber. The argon gas plasma source ionizes argon gas with a radiofrequency coil to produce a high-temperature plasma. The sample is heated by the plasma to extremely high temperatures (about 10000 K), which causes the molecules to separate into atoms and ions. The spectrophotometer is able to collect the light emitted by atoms and ions in the plasma at the characteristic wavelength. Then, the light is separated into individual wavelength with a diffraction grating or prism and its intensity is

measured by the detector and converted into a spectrum. The concentration of elements in the sample can be calculated from the spectrum produced by the ICP-OES equipment, comparing the intensity of the emission at the characteristic wavelength of the element to a calibration curve generated using standard solutions of known concentration. In this project, inductively coupled plasma-optical emission spectrometer (ICP-OES) (Agilent Scientific Instruments, Headquarters, Santa Clara, CA, United States) instrument was used to detect the amount of silver nanoparticles on the catalyst with argon as a carrier gas.

2.2.4 Fourier Transform Infrared spectroscopy (FT-IR)

FT-IR spectroscopy is a technique used to obtain information about the vibrations of molecular bonds in a material. Different chemical bonds absorb infrared radiation at specific frequencies, therefore by analyzing the frequencies of infrared radiation that are absorbed by a sample, FT-IR spectroscopy can provide information about the chemical composition and structure of the sample. FT-IR spectrophotometer comprises the source, the interferometer, and the detector. The technique is based on the use of an infrared beam, which moves through the sample such that some of the infrared energy is absorbed by the chemical bonds. The infrared beam reaches a detector, that measures the intensity of the radiation passing through the sample. The infrared beam is divided into two equal-intensity beams by the interferometer: one is directed into the sample and the other surrounds it. Then, the two beams are recombined and directed towards the detector. The intensity of the beam at each frequency and an interference pattern, created by the difference in the path length of the two beams, are used to calculate the absorption spectrum of the sample. The instrument used in this work for the analysis of the catalyst was Bruker Vertex 80 FT-IR spectrometer in the range between 500 and 4000 cm^{-1}.

2.3 Experimental procedures

All the experimental procedures applied for the catalyst synthesis are explained in this section.

2.3.1 Catalyst synthesis

Catalyst synthesis can be divided into two different steps: the preparation of chitosan-substrate and silver nanoparticles production, and their loading on the support.

2.3.1.1 Chitosan support preparation

The catalyst was prepared following the method in a previously reported article (Sargin, 2019). The chitosan (0.250 g) was mixed with an aqueous solution of acetic acid solution (12.5 mL, 2wt% acetic acid in water) and maintained under stirring for 24h to obtain a homogenous solution. The chitosan solution was further mixed with an aqueous alkaline solution for its neutralisation as well as precipitation. An alkaline solution was initially prepared with H_2O (17 mL), MeOH (25 mL) and NaOH (5 g). The homogeneous solution of chitosan was slowly added to the alkaline solution and formation of pale-yellow coloured beads took place. The reaction mixture was kept at room temperature for 24h to ensure complete coagulation of the beads. Following the alkaline treatment, the sample was rinsed and filtrated, until a neutral pH was reached. For cross-linking of chitosan, the beads were mixed with a solution prepared from methanol (6 mL) and aqueous solution of glutaraldehyde (0.1 mL, 50 wt.% in water). The reaction mixture was refluxed for 6 hours at 70°C using a water bath. Following this procedure, beads were separated from the reaction mixture by vacuum filtration and washed with a mixture of ethanol and water (40 mL H 2O, 40 mL EtOH). The obtained solid was the freeze dried overnight and stored at dry conditions prior to analysis and catalyst synthesis. The recovery of the chitosan after crosslinking method was calculated by equation 2.4, where $m_{recovered\ chitosan}$ is the amount of recovered solid after crosslinking (g) and $m_{initial\ chitosan}$ is the amount of chitosan used at the beginning (g).

$$\%\ recovery = \frac{m_{recovered\ chitosan}}{m_{initial\ chitosan}} \cdot 100 \qquad (2.4)$$

2.3.1.2 Synthesis of silver nanoparticles on chitosan support

The silver nanoparticle loaded catalysts were obtained by using $AgNO_3$ as a metal precursor and cross-linked chitosan. The cross-linked chitosan (0.217 g) was mixed with a freshly prepared solution of silver nitrate in water (10 mL H_2O, 0.04 g $AgNO_3$) and reaction mixture was stirred at 70°C for overnight using an oil bath. After processing overnight, the colour of the solid sample changed into a dark brown one, indicating the deposition of silver metal on the chitosan surface. The sample was washed with distilled water (50 mL), filtered by vacuum filtration and dried by freeze drying.

2.3.2 Vacuum filtration

A typical laboratory method for separating solids from liquids is vacuum filtration. There are some important parts that must be present in a setup used for the filtration in vacuum: filter paper, buncher funnel, filter adapter, filtering flask, vacuum hose and vacuum pump (Figure 2.4). During the process, the filter paper has to be placed in the funnel as close as possible to fit the funnel itself. Then, the filter adapter is inserted in the flask, while the funnel in placed in the stopper. The side spout is connected through a tube to the vacuum pump. The filter paper must be moisten with the same solvent or liquid of the sample under study because it creates an air-tight seal between the filter paper and the funnel, preventing any contamination. When the vacuum pump is turned on, the solution has to be placed in the funnel and in this way the solids can be collected on the top of the filter paper, while the solvent goes down and it is captured in the filtering task. The filter paper is chosen depending on the size of solids particles being filtered, and it needs to be chemically compatible with the solvent and the particles. Vacuum filtration can speed up filtration, but too much suction can pull too strongly or harm the paper. In this work, vacuum filtration was used during both catalyst support preparation and silver nanoparticles synthesis on chitosan support. After filtration, samples were separated from the solution, but they needed be dried because a lot of water was still present. Therefore, drying was carried out after each filtration step.

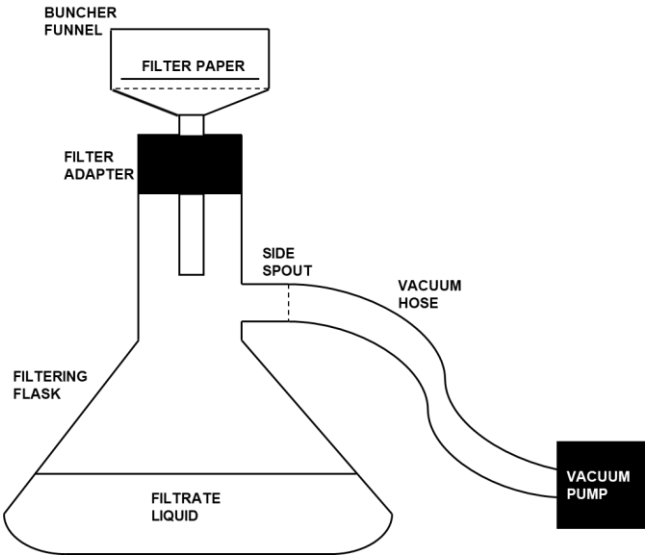

Figure 2.4 - Scheme of vacuum filtration setup

2.3.3 Freeze drying

Freeze drying is a process in which a completely frozen sample is placed under vacuum to remove water or other solvent from a sample, allowing the ice to change directly from a solid to a vapor, without passing through a liquid phase. Thus, a sublimation occurs. In this way, the properties and the chemical structure of the sample are preserved. The sample needs to be completely frozen, usually below its triple point. A vacuum chamber, a condenser, and a refrigeration system are often used as equipment for freeze drying. Once the sample is properly frozen, it is placed on the machine and the sublimation starts. Depending on the type of sample and the amount of heat applied, it may take several days. The material is placed under vacuum and gradually heated. The sublimation of the frozen water molecules occurs as the temperature rises and this is feasible thanks to the reduction of pressure, which allows faster ice evaporation. The water vapor is finally removed from the vacuum chamber during the desorption step by condensation, absorption on a cold surface, or employing a dry gas stream. The final material, in a dry and porous form, is obtained, keeping its shape and structure. The instrument used in this study to carry out freeze drying was Scanvac CoolSafe Freeze Dryer (Figure 2.5A).

Figure 2.5 - A) Scanvac CoolSafe Freeze Dryer; B) Dewar flask with round-bottomed flask containing hydrogel chitosan beads and water; C) Dewar flask

This process was used during support preparation to dry hydrogel chitosan beads because drying cannot be done with a simple oven, since chitosan needs to preserve its high surface area that can be damaged with high temperature. For the same reason, freeze drying was applied also during the synthesis of silver nanoparticles. After filtration, hydrogel chitosan beads were mixed with distillate water in a round-bottomed flask, that was placed inside a Dewar flask

(Figure 2.5B). It is an insulating storage vessel and consists of two flasks, one within the other, and the gap between them is partially evacuated of air, creating a near vacuum which reduces the heat transfer through convection or conduction (Figure 2.5C). Dry ice and acetone were placed inside this vessel to obtain a very cold liquid able to completely freeze the sample. Then, the sample was placed in the freeze dryer for 24h or more, until it was completely dried.

2.3.4 Preparation of catalysts with different loading of silver nanoparticles

Other two catalysts were prepared following the method previously explained, but with different amount of $AgNO_3$. The support used in this case was the same, but changing the quantity of silver nitrate, also the amount of silver nanoparticles loaded on the support changed. Totally, three different catalysts were prepared: 0.150 g of cross-linked chitosan were mixed with a freshly prepared solution of silver nitrate in water (7 mL), in which 0.005, 0.02 or 0.04 g of metal precursor was used. The catalysts are here onwards designated as catalyst 1, catalyst 2 and catalyst 3 in upcoming descriptions regarding their characterizations and catalytic testing. The wt.% of $AgNO_3$ used for the preparation of the three catalysts sample was computed with Equation 2.5.

$$wt.\%\ of\ AgNO_3\ in\ catalyst\ synthesis = \frac{m_{AgNO_3}}{m_{chitosan} + m_{AgNO_3}} \cdot 100 \qquad (2.5)$$

First, the total mass of the sample, namely $m_{total} = m_{chitosan} + m_{AgNO3}$, was calculated. Then, introducing the molecular weight of silver and silver nitrate ($MW_{Ag} = 107.86\ g{\cdot}mol^{-1}$; $MW_{AgNO3} = 169.87\ g{\cdot}mol^{-1}$), the amount of Ag in $AgNO_3$ was quantified using Equation 2.6.

$$m_{Ag}\ in\ AgNO_3 = m_{AgNO3} \cdot MW_{Ag}/MW_{AgNO3} \qquad (2.6)$$

The theoretical wt.% of Ag on the catalyst was finally obtained as follow:

$$theoretical\ wt.\%\ of\ Ag = \frac{m_{Ag}\ in\ AgNO_3}{m_{total}} \qquad (2.7)$$

Table 2.2 shows all the results of the described calculations for the three catalysts. An important aesthetic difference among the three catalyst was the colour: the more the silver, the browner the sample (Figure 2.6).

***Table 2.2**. Total amount of sample, amount of $AgNO_3$, amount of Ag in $AgNO_3$ and theoretical wt.% of Ag on chitosan sample computed according to Equation 2.7 for the three different catalysts*

	m_{total} [g]	$m_{chitosan}$ [g]	m_{AgNO3} [g]	m_{Ag} in $AgNO_3$ [g]	theoretical wt.% of Ag	%wt of $AgNO_3$ used in the catalyst synthesis
Catalyst 1	0.155	0.15	0.005	0.00317	2.045	3.2
Catalyst 2	0.17	0.15	0.02	0.0127	7.47	11
Catalyst 3	0.19	0.15	0.04	0.0254	13.37	21

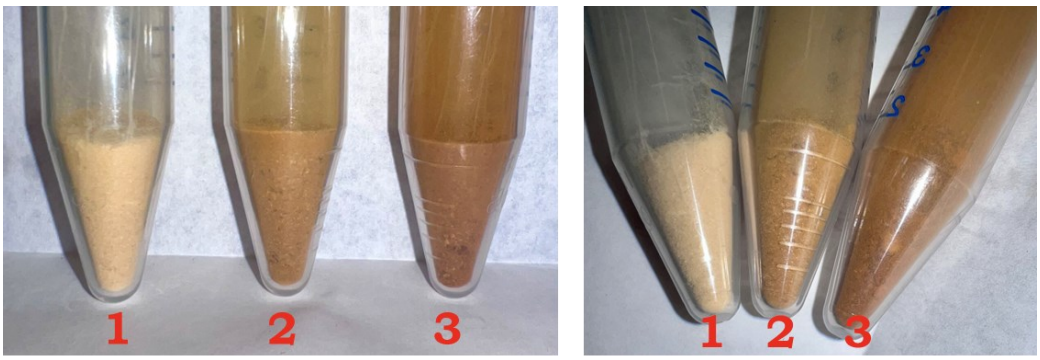

Figure 2.6 - Ag/CH catalysts prepared with 1) 0.005 g of AgNO3, 2) 0.02 g of AgNO3, 3) 0.04 g of AgNO3

2.4 Determination of silver loading on chitosan surface using ICP-OES

ICP-OES was used to determine the actual wt.% of Ag on the catalyst sample and compare it with the theoretical values. The amount of silver on chitosan surface was measured for the three different catalysts with different metal loadings, for the chitosan support and the recycled catalyst 3. The catalysts were initially digested with concentrated nitric acid (1 mL, 65% HNO_3) for 5-6 hours at 90°C. Then, catalysts were separated by filtration and obtained filtrate was

diluted with an appropriate amount of HNO_3 solution (2.5%) and water. Prior to measurement of amount of Ag in catalysts, the calibration curve with different concentrations of silver was prepared. Standard solutions with specific concentration of Ag were made, and then, during measurements, different intensities of lights were obtained for each isotope of silver (Ag 328, Ag 338, Ag 420). The correct one was chosen (Ag 328), and the curve of concentration Vs intensity was generated using Excel (Figure 2.7).

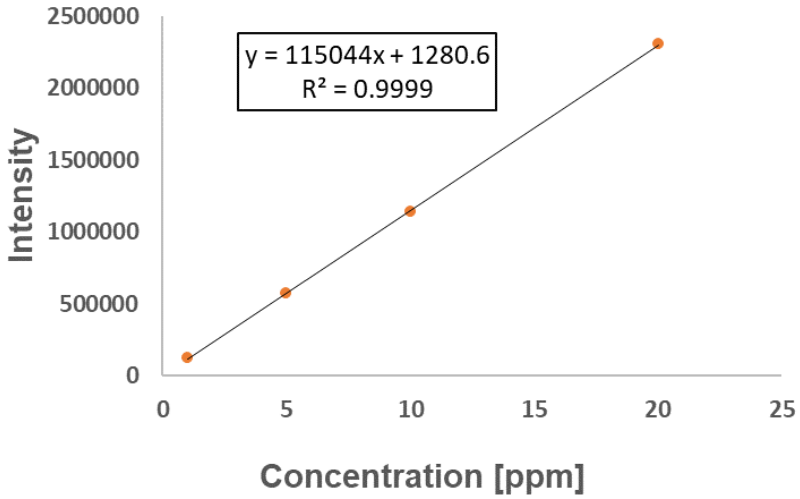

Figure 2.7 - Calibration curve of intensity vs. concentration obtained from standard solution of Ag

Once the calibration curve and the corresponding equation were obtained, concentration values of silver on each catalyst sample were retrieved. From the ICP-OES analysis, data on intensity for each sample were acquired, therefore the analysis of catalysts was preceded where concentration (in ppm) of Ag in each catalyst was obtained with the calibration curve. Since for each catalyst dilution volume and amount of sample were different, the wt.% of Ag in each catalyst calculated with Equation 2.8.

$$\%Ag = \frac{c_{Ag} \cdot V_{dilution}}{m_{sample}} \cdot 100 \qquad (2.8)$$

In equation 2.8, c_{Ag} is silver concentration in ppm, $V_{dilution}$ is the volume (in mL) used to dilute the sample after digestion with concentrated nitric acid, and m_{sample} is the amount of catalyst sampled for the analysis in µg.

Table 2.3 - Actual wt.% of Ag in catalyst 1, catalyst 2 and catalyst 3

	Measured wt.% of Ag	**Actual wt.% of Ag**
Chitosan support	0.1	-
Catalyst 1	1.5	1.4
Catalyst 2	4.5	4.4
Catalyst 3	6.8	6.7
Recycled catalyst 1	6.2	6.1

Since a small amount of silver was already present in the chitosan support, the actual wt.% of Ag in each catalyst was evaluated by subtracting the wt.% of Ag in chitosan support from each value computed with Equation 2.8 (Table 2.3).

Chapter 3
Catalyst characterization and catalytic activity

This chapter is dedicated to Ag/CH catalyst characterization through XRD, SEM and FT-IR, and the catalytic activity of the catalyst through the organic transformation of p-nitroaniline and phenol red dye.

3.1 Catalyst characterization

3.1.1 XRD

X-Ray powder Diffraction (XRD) technique was used to determine the active phase of the catalysts, determine the crystal structure, and identify the active phases. Crosslinked chitosan support and the three synthesized catalysts were analyzed and results were compared. XRD patterns are shown in Figure 3.1. According to literature, chitosan can have two crystalline structure, described by two crystalline peaks at 2θ = 10.3 and 20.1°, corresponding to the (010) and (110) diffraction plane, respectively (Wegrzynowska-Drzymalska *et al*., 2020). The cross-linked chitosan showed diffraction peak at 2θ value around 21° regarding to (110) plane, while peak at 10.3° was not observed. This can be associated to a decrease of crystallinity of chitosan because of chemical treatments, therefore the hypothesis is that the glutaraldehyde-induced crosslinking process increases the amorphous portion of the chemical structure (Sencadas *et al*., 2012). In the case of catalysts, diffraction peak at 2θ value of 21° was still present, but as the amount of Ag metal increased, it was steadily decreasing and the lowest value was observed with catalyst 3, due to possible covering with silver nanoparticles. Hamzavi *et al*. (2018) reported that peaks at 2θ = 37.97°, 44.05°, 64.21° and 77.25° were associated with (111), (200), (220), and (311) planes of face-centered cubic Ag crystals. In the analysed samples, it was observed the peak at 2θ value 37.97° for Ag metal only in the case of catalyst 3. However, this peak was not observed for the catalyst 1 and 2, probably dye to the low concentration as well as the homogeneous distribution of Ag metal on the catalyst surface.

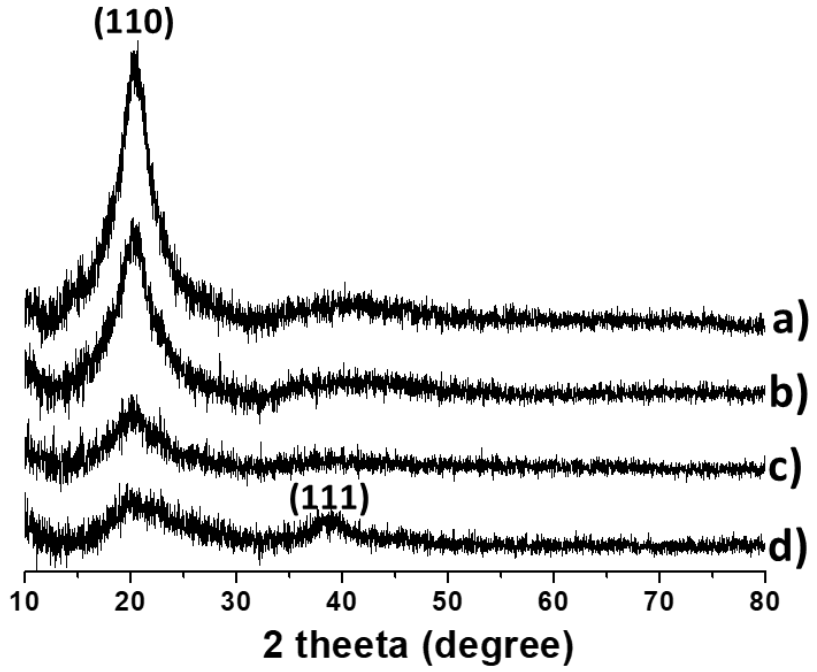

Figure 3.1 - XRD pattern of a) cross-linked chitosan b) Ag/CH catalyst 1 c) Ag/CH catalyst 2 d) Ag/CH catalyst 3

3.1.2 FT-IR

Fourier transform infrared spectroscopy (FT-IR) was used to identify different functional groups in neat and cross-linked chitosan and catalyst 3 to understand the structural changes in chitosan after cross-linking and Ag metal loading. Regarding spectra are shown in Figure 3.2. The neat and partially deacetylated chitosan shows a stretching vibration band at 1650 cm^{-1} belonging to C=O (amide I) due to acetyl groups of chitin still present in chitosan, and 1550 cm^{-1}, corresponding to N-H (amide II) stretching vibrations in amide group (Frick *et al*., 2018). Another vibration bands at 1585 cm-1 for N-H stretching vibrations can be noticed (Hamzavi *et al*., 2019). The bands for the stretching vibration of C-N bond were observed between 1376 and 1255 cm^{-1} while the bands belong to the 1, 4-glycosidic bond (C-OC) as well as C-O bond in the secondary (C3) and primary (C6) -OH groups of chitosan appearing at 1150, 1060 and 1025 cm^{-1}, respectively. After cross-linking with glutaraldehyde, the band attributed to N-H stretching vibrations in amine disappeared, while the band representing the stretching vibrations

in C=N bond at 1650 cm^{-1} appeared. This is an evidence that crosslinking took place, since C=N bond occurred between the amine groups of chitosan and the carbonyl groups of glutaraldehyde. (Sencadas *et al*., 2012, Frick *et al*., 2018). This newly formed band is overlapped with band representing amide I functional group (C=O in amide group), hence the overall intensity of the band increased. It was not observed a significant change in the functional groups after Ag metal loading, except the increase in the intensity of the band corresponding to C-N stretching vibrations. Shifting of the peaks can be linked to interaction between silver and chitosan.

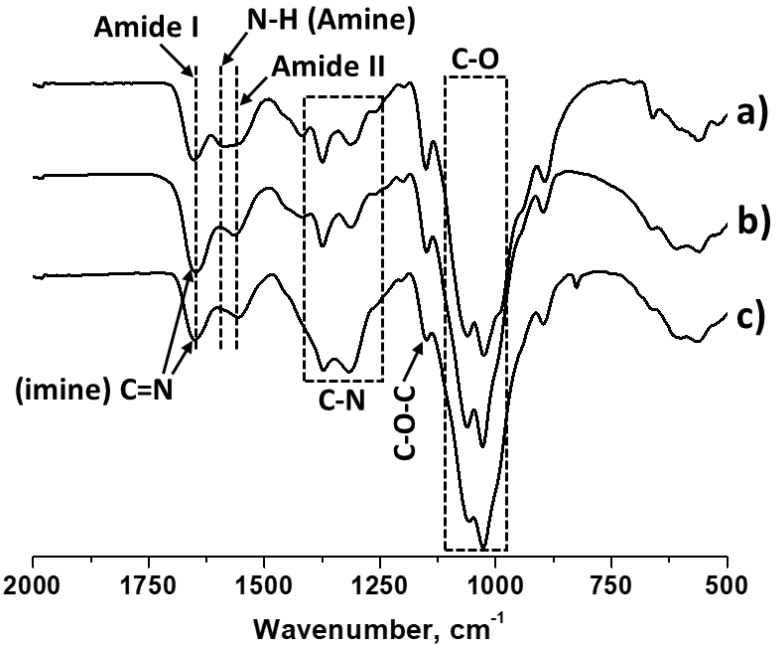

Figure 3.2 - FT-IR spectrum of a) neat chitosan, b) crosslinked chitosan c) catalyst 3

3.1.3 SEM and SEM-EDX

The surface morphology of cross-linked chitosan and Ag/CH catalysts with different loading of Ag was studied using Scanning electron microscopy, while their chemical composition was obtained with scanning electron microscopy with EDX analysis. Corresponding images and spectra are shown in Figures 3.3 and 3.4, respectively. The SEM images show that material with a rough surface was obtained after the cross-linking of the chitosan with glutaraldehyde

while materials with identical morphology were obtained after various amount of silver loadings. Thus, silver does not influence morphology of the catalyst, probably due to its low concentration. On the other hand, the SEM-EDX analysis confirms the deposition of the Ag metal over the chitosan support. Comparing cross-linked chitosan with catalysts spectra, it is evident the presence of Ag in Ag/CH catalysts, with an apparent increase of the peak increased with metal loading (Figure 3.4).

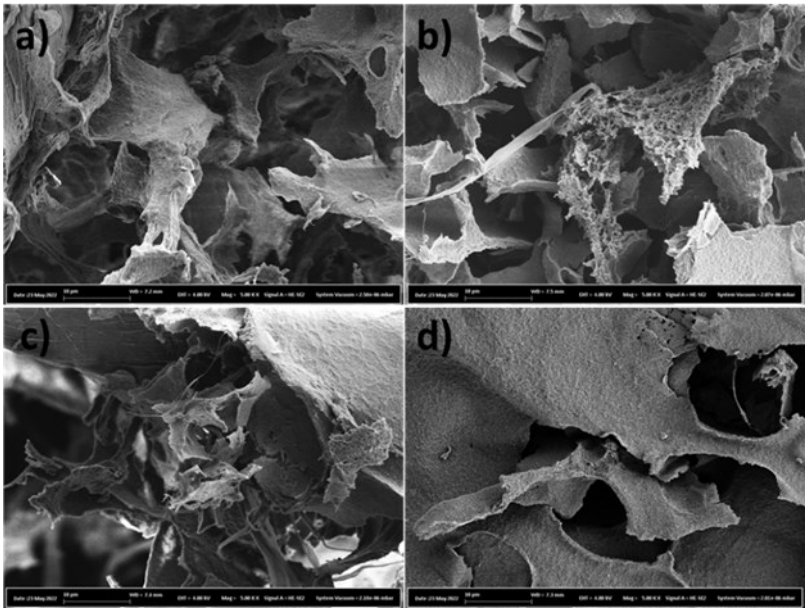

Figure 3.3 - SEM images of a) cross-linked chitosan, b) Ag/CH catalyst 1, c) Ag/CH catalyst 2 and d) Ag/CH catalyst

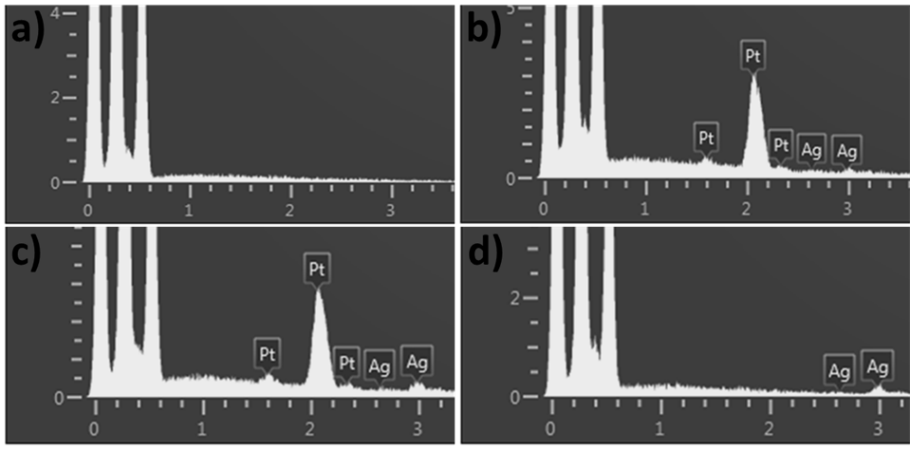

Figure 3.4 - SEM-EDX spectrum of a) cross-linked chitosan b) Ag/CH catalyst 1, c) Ag/CH catalyst 2 and d) Ag/CH catalyst 3

3.2 Assessment of the catalytic activity

Catalytic activity of Ag/CH was tested in batch systems. Laboratory test tubes were used, where the catalyst and hydrogen source were charged; then, 2 mL of reacting solution was loaded in the test tube. A magnetic stir bar of proper dimensions was used to get the proper mixing conditions. The test tube was loaded into a magnetic block, which was placed on a magnetic stirrer with a heating plate to keep the desired temperature and mixing speed. Tools used for the experiments are showed in Figure 3.5.

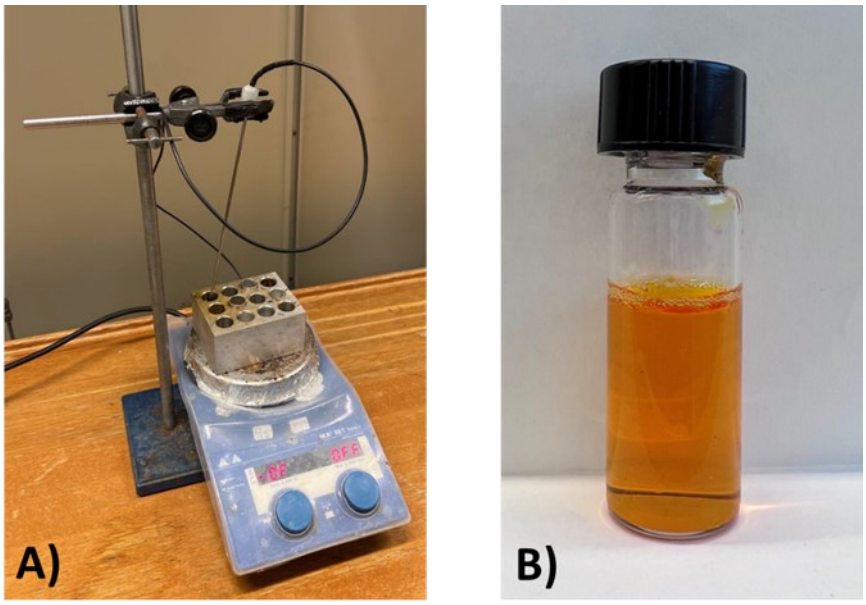

Figure 3.5 - A) Magnetic stirrer with heating plate; B) Laboratory test tube filled with phenol red dye solution

3.2.1 Reduction of p-nitroaniline with chitosan supported Ag catalyst

According to Sargin's work (2019), chitosan supported silver catalysts is useful for the reduction of nitroaromatic compound, therefore the Ag/CH is tested with p-nitroaniline (PNA). By reducing PNA, in which nitro group ($-NO_2$) is reduced to amino group ($-NH_2$), p-phenylenediamine (PPD) is obtained as product (Figure 3.6). PNA sample was prepared by dissolving the powder into distillate water to get an aqueous solution 0.001 M. Initially, the experiments were done taking 2 mL of PNA solution 0.001 M and mixing it with 5 mg of $NaBH_4$, which is the hydrogen sources for the reduction, and 6 mg of Ag/CH catalyst 3,

resulting in 2.5 and 3 mg mL^{-1} in concentration, respectively, under constant stirring (500 rpm) and room temperature (20°C). The treatment of the deep yellow PNA with the mixture of $NaBH_4$ and Ag/CH caused the color of the solution to start fading, and in about 6 minutes the solution turned clear and colorless (Figure 3.7). This could be considered as an indication that reduction occurred.

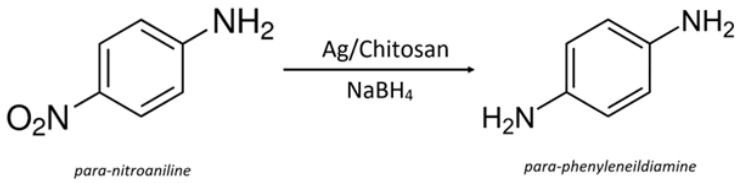

Figure 3.6 - Scheme of PNA reduction

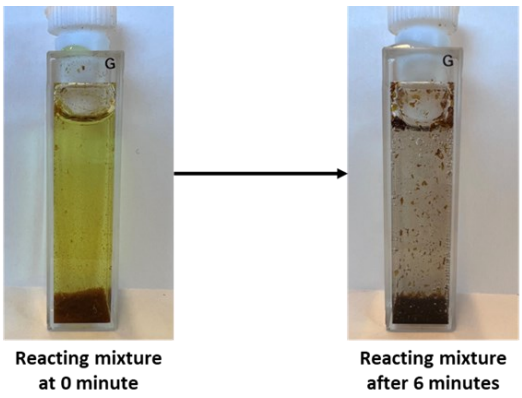

Figure 3.7 - Reacting mixture of PNA with $NaBH_4$ and Ag/CH catalyst

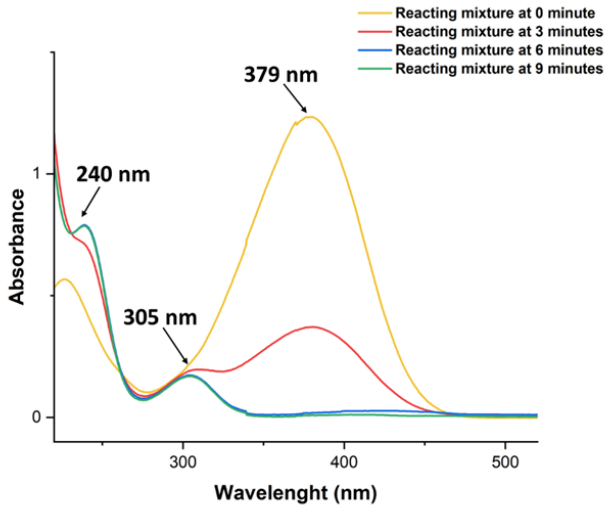

Figure 3.8 - UV spectra of 0.001 M PNA solution during reaction with 5 mg of $NaBH_4$ and 6 mg of Ag/CH

To evaluate the progress of reaction, the UV-vis spectrophotometer was used, using the procedure described in Chapter 2. The characteristic wavelength for the PNA is 379 nm and at 0 minutes there is a max value for the absorbance, at this wavelength. Once the reaction started, this peak started decreasing, until the complete disappearance was achieved. As the reduction progressed, it was possible to notice the appearance of two different peaks, respectively around 240 nm and 300 nm: they are characteristic of the final product of the PNA reduction, namely PPD (Figure 3.8).

Different studies were done to demonstrate Ag/CH effectiveness for the reduction of PNA. The reaction was tested in different conditions, changing one parameter and keeping the other constant. Several experiments were carried out, changing the amount of catalyst, the amount of $NaBH_4$, the concentration of PNA and the temperature. Furthermore, different catalysts with different loading of silver nitrate were tested, to evaluate the importance of the silver nanoparticles on catalyst. Finally, the catalyst was tested to verify its reusability.

3.2.1.1 Effect of catalyst concentration

The concentration of Ag/CH in the reacting mixture is an important factor that can impact the rate at which PNA is catalytically reduced. The progress of reduction of PNA was monitored with different concentration of catalyst 3 such as 3, 2, 1 or 0.5 mg mL^{-1} and 2.5 mg mL^{-1} of $NaBH_4$. As shown in Figure 3.9A, it was observed that the reduction capacity of the catalyst decreased with its concentration. After 6 minutes, PNA had completely converted into PPD with the higher amount of catalyst, while when using 2, 1 and 0.5 mg mL^{-1} of Ag/CH catalyst, complete conversion was achieved in 9, 18 and 21 minutes, respectively. To confirm the results and verify that only with the catalyst reaction occurred, an attempt with only reducing agent and reactant was done. Considering the same reducing time, no reaction occurred. Thus, the simultaneous presence of $NaBH_4$ and Ag/CH is fundamental because reduction do not take place with only $NaBH_4$, therefore the use of the catalyst is necessary.

3.2.1.2 Effect of $NaBH_4$ concentration

In Figure 3.9B, the percentage conversion of PNA into PPD is analyzed with different concentrations of $NaBH_4$. It was used as hydrogen source in the reduction and its amount can influence the progress of the reaction. The catalytic reduction was performed at room

temperature using 3 mg mL^{-1} of catalyst 3 and various concentrations of $NaBH_4$ such as 2.5, 1.25, or 0.5 mg mL^{-1}. The percentage of conversion decreases as the concentration of $NaBH_4$ decreases. It was observed that even with the lowest concentration of hydrogen source (0.5 mg mL^{-1}), PNA conversion reached about 85%. Many studies report chitosan as a good absorbent for a wide range of organic compounds (Jiménez-Gómez and Cecilia, 2020). Therefore, an experiment without $NaBH_4$ was carried out. However, the reacting system remained unchanged and PNA concentration was unaltered after 12 minutes when only catalyst was used. Absorption did not take place, thus the use of Ag/CH alone for the removal of PNA is not effective and a reducing agent is needed.

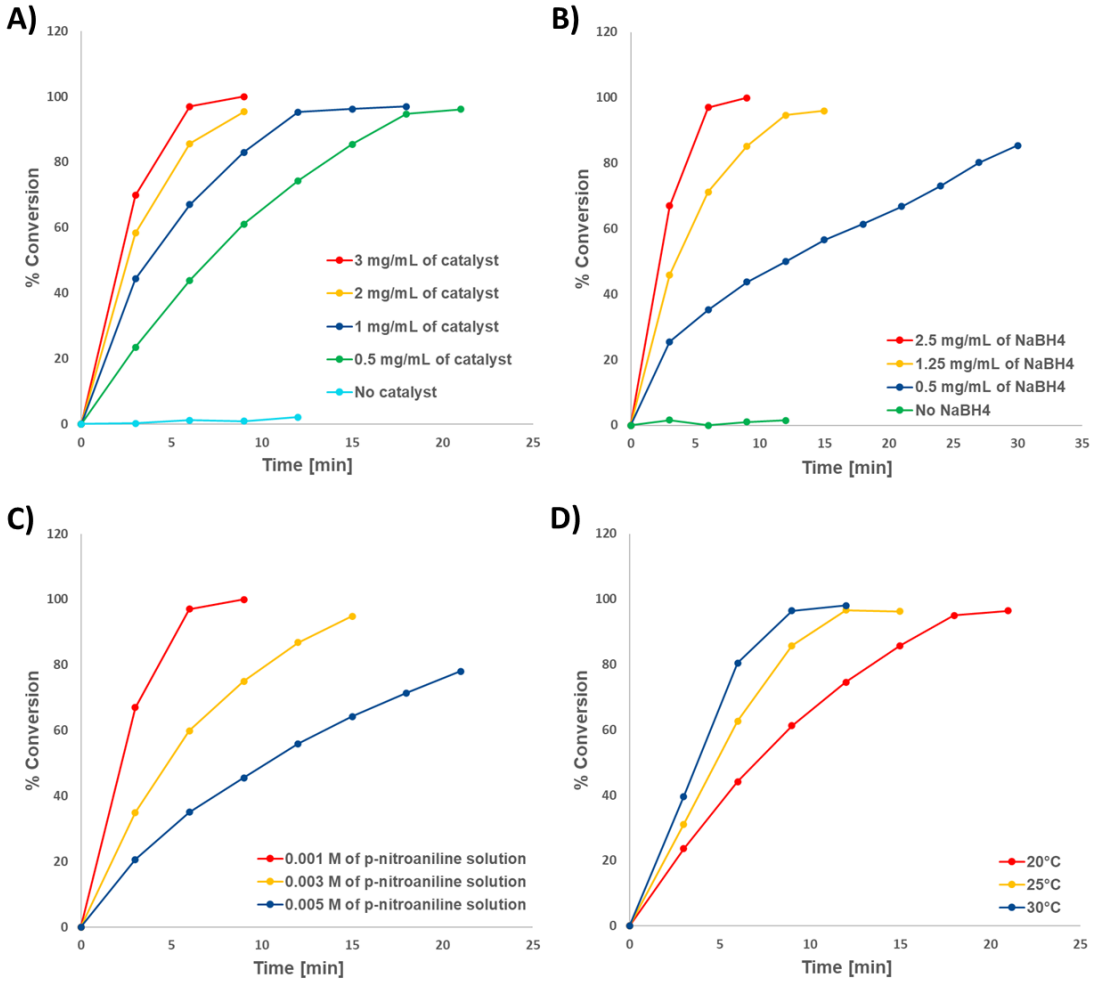

Figure 3.9 - Reduction with A) different concentration of catalyst 3 and 2.5 mg mL^{-1} of $NaBH_4$, 2 mL of PNA solution (0.001 M), 20°C, B) different concentration of $NaBH_4$ and 3 mg mL^{-1} of catalyst 3, 2 mL PNA solution (0.001 M), 20°C, C) different concentration of 2 mL of PNA solution and 3 mg mL^{-1} of catalyst 3, 1 mg·mL^{-1} of $NaBH_4$, 20°C, D) different temperature and 0.5 mg mL^{-1} of catalyst 3, 2.5 mg mL^{-1} of $NaBH_4$, 2 mL of PNA solution (0.001 M)

3.2.1.3 Effect of p-nitroaniline concentration

Different PNA aqueous solution were prepared to evaluate the behaviour of Ag/CH catalyst with different concentration of the reactant, such as 0.003 M and 0.005 M. The 0.001 M solution took 6 minutes to convert PNA completely, the 0.003 M solution took 15 minutes to obtain a percentage of conversion of 95% and 0.005 M solution required 21 minutes to get only 78% of conversion (Figure 3.9C). The increase of concentration may require higher amount of catalyst because the active sites are not enough.

3.2.1.4 Effect of temperature

The reaction mixture was tested also at different temperatures, namely 25°C and 30°C, and results were compared with previous experiments at room temperature (20°C) to better understand the impact of temperature on the rate of reaction. During temperature studies, the concentration of catalyst was decreased to 0.5 mg mL^{-1} since the reaction rate was too high when 2.5 mg mL^{-1} of $NaBH_4$ and 3 mg mL^{-1} of catalyst were used at room temperature. The progress of conversion is showed in Figure 3.9D. As the reaction temperature was raised from room temperature to 25 and 30°C, the rate of the reaction increased significantly.

3.2.1.5 Effect of different type of catalyst

As silver nanoparticles represent the active sites where reactions occur, their loading is a significant factor that can alter the rate at which PNA is reduced. Thus, various catalysts, including 1, 2, and 3, with various Ag metal loadings, were utilized, and the effect of metal loadings on reaction rate was investigated. As more Ag metal was loaded on each cross-linked chitosan support, the rate of reduction increased progressively: it was observed that with catalyst 2 and catalyst 3 in almost 6-9 minutes, a complete conversion was obtained, while catalyst 1, which is characterized by lower Ag nanoparticles, required 24 minutes to reach a conversion of 90% (Figure 3.10A). The number of sites on the catalyst surface that are active grows as the silver concentration rises, and the result is an increase in the conversion percentage estimated over time.

3.2.1.6 Reusability of catalyst

One of the major advantages of using Ag/CH as a catalyst for PNA reduction is the possibility

to reuse it. It is a heterogenous catalyst, for which the separation from the reagent solution turns out to be very simple, such that its reuse is feasible. Therefore, it is very important to measure the possible deactivation of Ag/CH catalysts over the time. The recyclability investigation for the PNA reduction process used the Ag/chitosan catalyst 3 with 6.7 wt.% Ag metal loading. The catalyst was separated and recycled 5 times, and ICP-OES analysis was used to examine the obtained recycled catalyst and any additional loss of Ag metal during the recycle investigation. The results of recycling are shown in Figure 3.10B. It was found that catalytic activity did not decrease, and catalyst behaviour was more or less the same across all of the recycle cycles. ICP-OES results demonstrated that the percentage of Ag loaded on chitosan support after 5 recycling step was similar to the fresh catalyst, because a value of 6.5 wt.% was obtained.

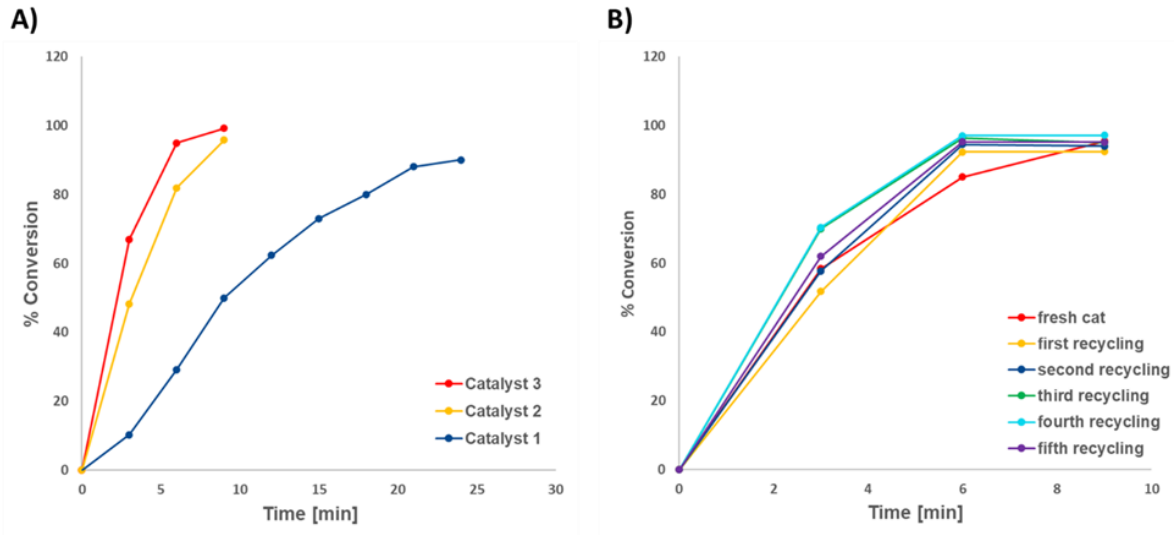

Figure 3.10 - (A) Reduction of 0.001 M PNA solution with different catalyst. (B) Comparison of reduction

3.2.1.7 Evaluation of intrinsic uncertainty of laboratory measurements

It can be presumed that the conversion curves over time with a fresh and recycled catalyst are equal (Figure 3.10B). It is reasonable to suppose that the catalyst is not changing because, if there were a trend, the fresh catalyst curve would have been above the first recycling curve, which in turn would have been above the third recycling curve, and so on. Since this scenario does not occur, it can be assumed that the observed data variability is exclusively due to

experimental reproducibility, namely the intrinsic uncertainty of laboratory measurements. It is clear from Figure 3.10B that the measurement at 6 minutes for the new catalyst is consistently lower than the same measurements for the recycled catalysts, indicating that this test is not representative of the 6-minute measurement. Additionally, it appears that the results at 3 minutes are more variable than those at 9 minutes, which is always a result of the intrinsic uncertainty in the experimental measurements. Based on these assumptions, it can be concluded that the catalyst does not lose its degradation ability. Therefore, Figure 3.10B contains duplicates of the same measurements, and using these data, it is possible to calculate the variability of experimental measurement, namely variance and standard deviation. For a population of measurements, the mean can be computed and each observation deviates from the mean. If the value of the observation is precisely the same as the mean, this deviation is 0. If the value of the observation is less than the average, the deviation will be negative. On the other hand, if the observation exceeds the average number, this deviation will be positive. To calculate the standard deviation, the squares of the deviations shall be used. The square enables the addition of negative and positive deviations without the outcome becoming null due to sign effects. Variance and standard deviation can be computed as reported in Equations 3.1 and 3.2, respectively.

$$\sigma^2 = \frac{\sum_{i=1}^{n}(x_i - \mu)^2}{n} \tag{3.1}$$

$$\sigma = \sqrt{\frac{\sum_{i=1}^{n}(x_i - \mu)^2}{n}} \tag{3.2}$$

In Equations 3.1 and 3.2, x_i is the value of a measurement, n is the number of measurements, μ is the average value of all experimental data and $(x_i - \mu)^2$ is the sum of all square average deviations. The variance is defined as the sum of the quadratic deviations (Equation 3.1). The square root with positive sign of variance is called standard deviation (Equation 3.2). Considering the experimental measurements of % conversion and concentration over the time in the case of recycled catalysts, variance and standard deviation were computed considering the tests at 3 minutes, since they are the one with higher variability. Results are shown in Table 3.1.

Table 3.1 *- Variance and standard deviation values computed for the experimental tests of % conversion and concentration of PNA reduction with recycled catalysts considering 3-minute measurements*

	σ^2	σ
% Conversion	45	6.7
Concentration [mol L^{-1}]	$4 \cdot 10^{-9}$	$6.3 \cdot 10^{-5}$

While the standard deviation has the same unit of measurement as the variable under analysis, the unit of measurement of variance is equivalent to the square of that unit of measurement.

3.2.1.8 Mechanism of reaction

A mechanism of catalytic reduction of PNA by $NaBH_4$ in presence of Ag/CH was elaborated (Figure 3.11).

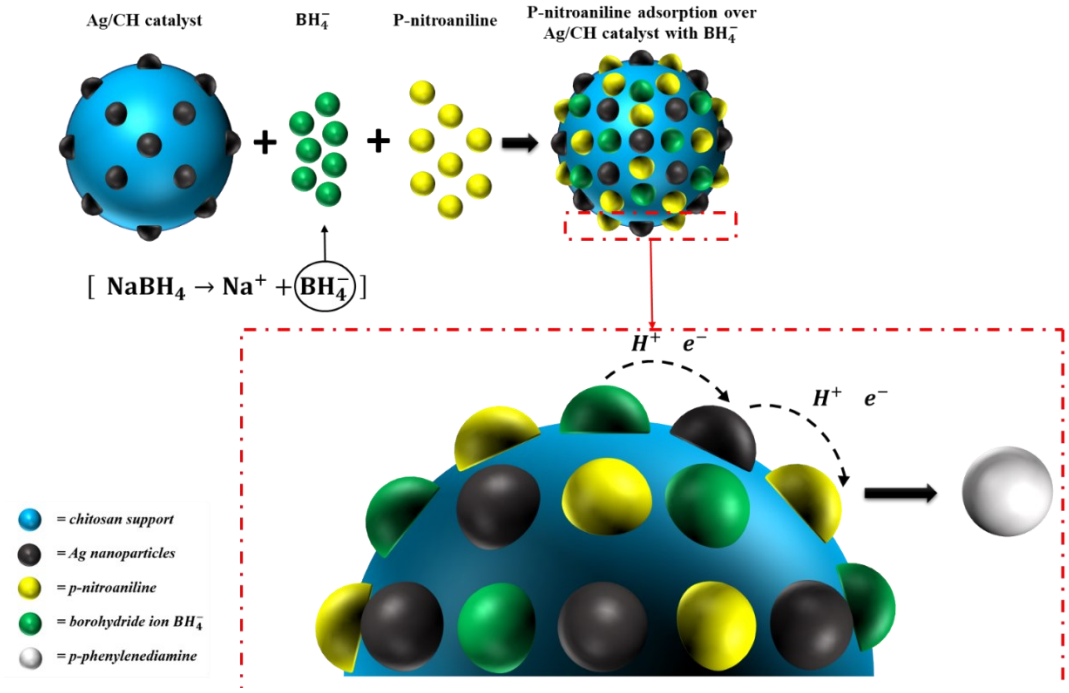

Figure 3.11 - Mechanism of p-nitroaniline reduction with NaBH4 and Ag/CH. Adapted from Naseem et al., 2018.

$NaBH_4$ dissociates in water and produces BH_4^{-1} ions, such that it works as hydrogen supplier and electron donor (Edison *et al*., 2016, Naseem *et al*., 2018). The mechanism can be seen as a series of subsequent steps. After their formation, BH_4^{-1} ions interact with the catalyst surface and stick to it and catalytic reduction starts thanks to the release of electrons by BH_4^{-1} to Ag

nanoparticles. On the other hand, PNA is also attached on the catalyst surface and it receives electrons from silver nanoparticles that have accepted them from BH_4^{-1} ions. BH_4^{-1} ions are able to transfer hydrogen to catalyst surface, and when PNA adsorbs on Ag/CH surface a complete reduction of PNA occur. The product is formed on Ag/CH surface and then it is released thank to diffusion (Edison *et al*., 2016).

3.2.2 Reduction of phenol red dye with chitosan supported Ag catalyst

The catalytic reduction of phenol red dye (PRD) was carried out with Ag/chitosan catalysts and $NaBH_4$ as the hydrogen source. The PRD solution was prepared by dissolving the powder of dye in distilled water to get an aqueous solution 0.001 M. Initially, the experiment was carried out by taking 2 mL of 0.001 M PRD solution, 5 mg of $NaBH_4$ and 6 mg of catalyst, resulting in concentration of 2.5 mg mL^{-1} and 3 mg mL^{-1} of $NaBH_4$ and catalyst, respectively. The reaction mixture was stirred (500 rpm), at room temperature (20°C). To evaluate the progress of the reaction, UV-vis spectrophotometry was used to monitor the progress of the reaction every 3 minutes. The catalytic activity of the catalyst was further evaluated under different reaction conditions where one reaction parameter was varied at the time.

3.2.2.1 Effect of pH

It was observed that after addition of Ag/chitosan catalyst and $NaBH_4$ in the red-orange colored PRD solution, the colour of the reaction mixture turned to pale fuchsia (colour in between pink and violet). As the reduction progressed, this colour slowly disappeared, and a colourless solution was obtained (Figure 3.12). As shown in Figure 3.13A, the 0.001 M red coloured aqueous solution of PRD gives rise to a peak with maximum absorbance at 436 nm. However, after addition of the catalyst and $NaBH_4$, and followed by proceeding of the reaction for 3 minutes, the peak at the 436 nm vanished while the peak with comparatively lower intensity appeared at 571.5 nm. The aqueous solution of phenol red is usually pH sensitive and it changes its colour. The aqueous solution of PRD shows yellow colour at acidic pH range, i.e. below pH 6.5, and orange-red colour in between pH 6.5 and 7.5, while it turns to fuchsia in alkaline pH range, i.e. above 7.5 (Chauhan *et al*., 2012, Held, 2018, Mittal *et al*., 2009).

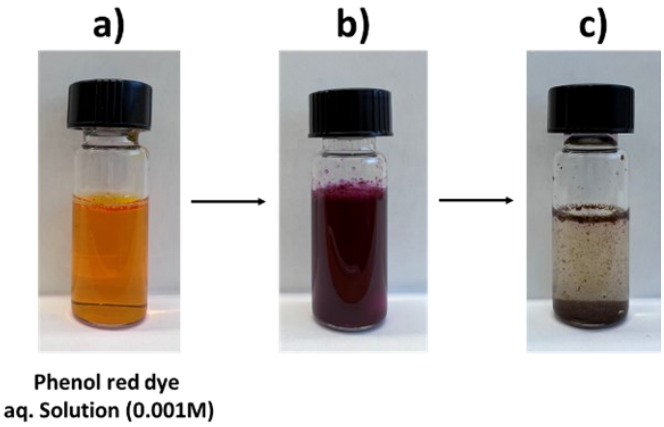

Figure 3.12 - a) PRD aqueous solution, Reaction mixture after b) addition of catalyst 3 and NaBH4 and c) complete reduction of PRD

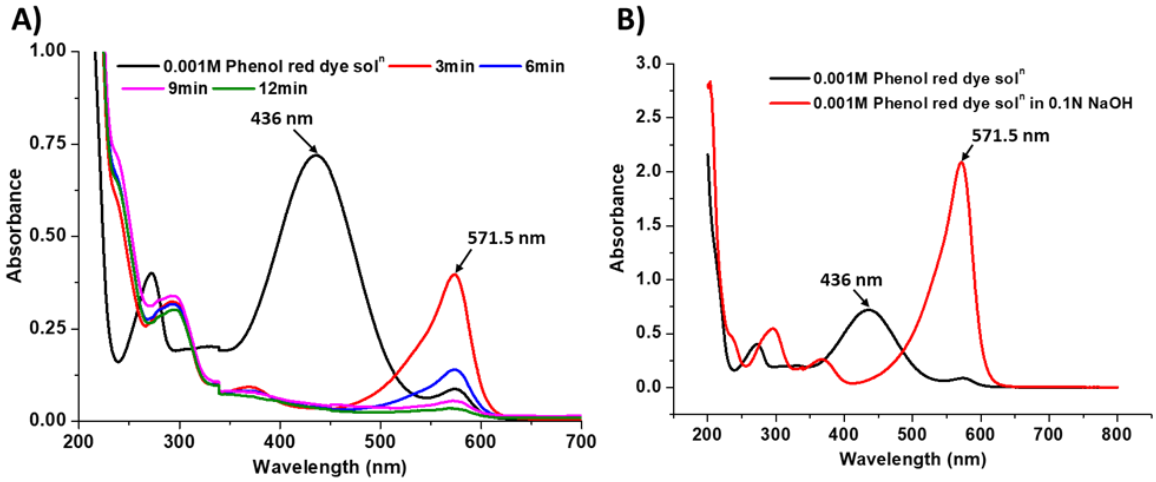

Figure 3.13 - (A) UV-vis spectra for the reduction of PRD by Ag/CH catalyst 3 (B) UV-visible spectra of 0.001M solution of PRD in distilled water and 0. 1N NaOH solution

Figure 3.14 shows the chemical structures of PRD in aqueous solution with different pH values where the dye gives rise to tautomeric and zwitterion form in high and moderately acidic pH range of the solution, respectively. At neutral pH, the PRD transforms to its phenol form whereas at alkaline pH, the phenate form of the dye remains dominant (Wahab *et al*., 2016, Held, 2018). In other words, the PRD forms variable molecular structures with different charge distributions depending on the pH of the solution where the -C=C- and -C=O chromophores in these structures impart different colour to the solution through extended conjugation. In the case of the catalytic process, since the colour of the reaction mixture changed to pale fuchsia after addition of catalysts and $NaBH_4$, it is assumed that the pH of the reaction mixture reached values higher than 7.5. The $NaBH_4$ usually undergoes decomposition in aqueous medium and

releases NaOH along with H_2 in aqueous solutions and the pH of the solution becomes alkaline (Reaction 3.3). To confirm this change in colour of reaction mixture with pH, the PRD solution was prepared in 0.1N NaOH solution and it was observed that the resulting solution become intense fuchsia in colour and the peak with at 571.5 nm was obtained upon UV-vis spectroscopic measurements (Figure 3.13B). Hence, this suggests that after the addition of the catalysts and $NaBH_4$, the tautomeric and zwitterion forms of the PRD were converted to their phenate analogue in alkaline medium. It was observed that as the reaction progressed, steady decolouration of reaction mixture occurred and simultaneously, the intensity of the peak at 571.5 nm also decreased. In this case, the conjugation in the PRD further terminated due to reduction of chromophores with Ag/chitosan catalyst and released H_2.

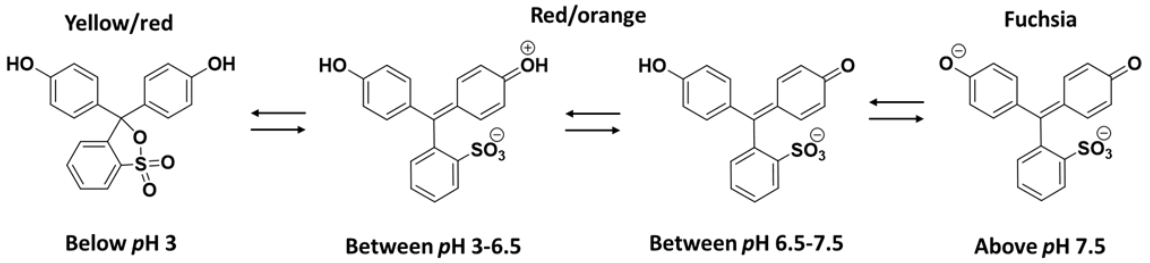

Figure 3.14 - Chemical structures of phenol dye in its aqueous solution with different pH conditions

$$NaBH_4 + H_2O \longrightarrow NaOH + H_2 + BH_3 \qquad (3.3)$$

Different reaction conditions were used to test the catalyst in the reduction of PRD, namely different catalyst amount, different amounts of hydrogen donor, different temperatures, and PRD concentration.

3.2.2.2 Effect of catalyst concentration

The influence of the catalyst concentration on the progress of reduction of PRD was confirmed where various concentration of catalyst 3 such as 3, 2, 1 or 0.5 mg mL^{-1} and 2.5 mg mL^{-1} of $NaBH_4$ were applied. As shown in Figure 3.15A, the reduction ability of the catalyst steadily increased with its amount. With 3 mg mL^{-1} of catalyst, a complete conversion of dye was obtained after 12 minutes while when using 2, 1 and 0.5 mg mL^{-1} of Ag/CH catalyst, complete conversion of the dye preceded in 12, 18 and 21 minutes, respectively. Furthermore, without

the catalyst, the rate of the reaction was decreased, but it is still quite significant; a small fraction of dye remained unconverted after 30 minutes of reaction. In this case, it is possible that Ag/CH was not required to reduce the dye; however, the reaction rate was lower compared to the catalytic reaction. Hence, this demonstrates that the catalyst is useful to induce an efficient reduction of a dye with $NaBH_4$.

3.2.2.3 Effect of $NaBH_4$ concentration

$NaBH_4$ was used as hydrogen source in the reduction of PRD. It releases NaOH in the reduction process of PRD and its amount can influence the progress of the reaction in terms of release of H_2 and pH of the reaction mixture, respectively. The progress of the reaction with different amounts of $NaBH_4$ is shown in Figure 3.15B. In this case, the catalytic reduction was carried out at room temperature where 3 mg mL^{-1} of catalyst 3 and different concentration of $NaBH_4$ such as 2.5, 1.25 or 0.5 mg mL^{-1} were utilized. The rate of reduction was decreased with the amount of $NaBH_4$ in the reaction mixture where nearly 60% of PRD was reduced in 30 minutes when 0.5 mg mL^{-1} of reducing agent was applied. However, without the reducing agent, the rate of discoloration of PRD was found high compared to reducing agent containing reaction mixtures where the colorless reaction mixture was obtained in 6 minutes (Figure 3.16a). As shown in Figure 3.16b, the catalyst with violet colour was obtained upon separation from the reaction mixture by filtration. This can be correlated to the adsorption of the PRD on the catalyst surface. With 2.5 mg mL^{-1} of $NaBH_4$ and after adsorption of dye over the catalyst, the reaction mixture turned to pale fuchsia while it further discolored in 15 minutes of reaction time.

3.2.2.4 Effect of phenol red dye concentration

The catalytic activity was further examined for the reduction of the PRD with different concentrations such as 0.001, 0.003 and 0.005 M in aqueous solutions where 3 mg mL^{-1} of catalyst 3 and 1.25 mg mL^{-1} of $NaBH_4$ were used. As shown in Figure 3.15C, the rate of reduction was varied with different concentrations of PRD solution. A complete conversion of dye was reached with the 0.001 M solution in 18 minutes, while upon use of 0.003 M and 0.005 M solutions, the 91% and 82% of conversion were achieved, respectively, in 30 minutes. As in the case on PNA, as concentration rises, more catalyst may be needed to increase the number of active sites and enhance a complete reduction of the dye.

3.2.2.5 Effect of temperature

The reaction temperatures during the reduction process were also varied to understand its effects on the progress of the reaction where the reaction mixture was heated at either room temperature (20°C) or 30 or 40°C, respectively. Since the reaction rate was high with 2.5 mg mL^{-1} of $NaBH_4$ and 3 mg mL^{-1} of catalyst 3, at room temperature, the concentration of $NaBH_4$ was reduced to 0.5 mg mL^{-1} during temperature study experiments. As shown in Figure 3.15D, the rate of the reaction was increased as the reaction temperature increased from room temperature to 30 and 40°C.

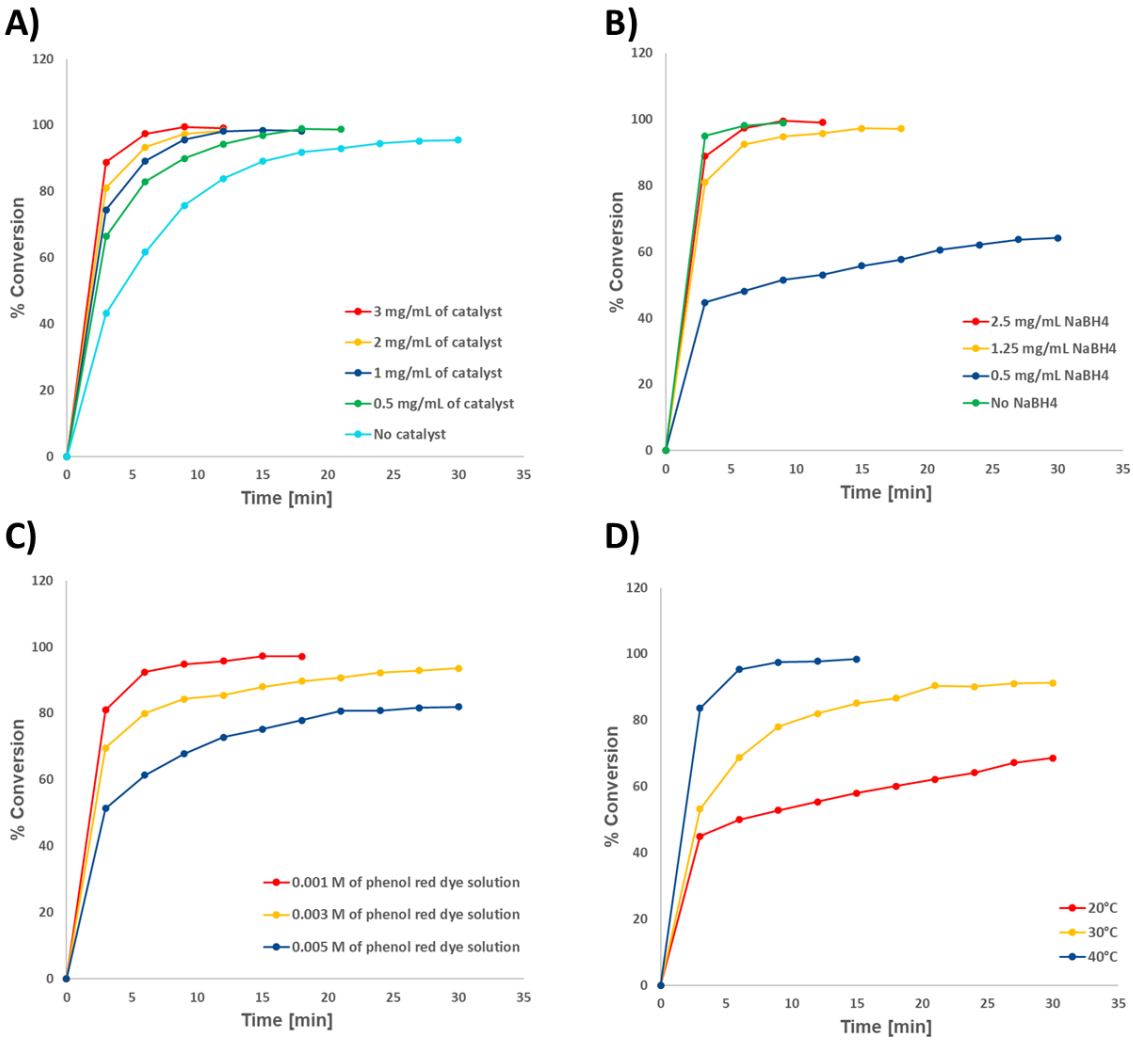

Figure 3.15 - Reduction with A) different concentration of catalyst 3 and 2.5 mg mL^{-1} of $NaBH_4$, 2 mL of PRD solution (0.001 M), 20°C, B) different concentration of $NaBH_4$ and 3 mg mL^{-1} of catalyst 3, 2 mL of PRD solution (0.001 M), 20°C, C) different concentration of 2 mL of PRD solution and 3 mg mL^{-1} of catalyst 3, 1.25 mg mL^{-1} of $NaBH_4$, 20°C, D) different temperature and 3 mg mL^{-1} of catalyst 3,0.5 mg mL^{-1} of $NaBH_4$, 2 mL of PRD solution (0.001 M)

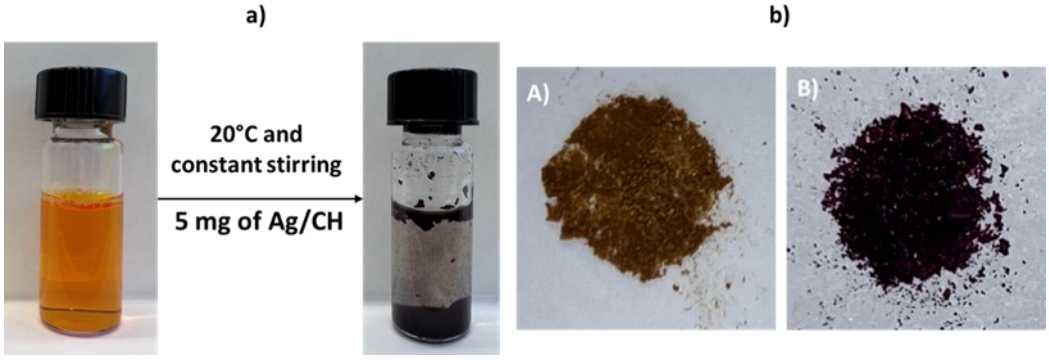

Figure 3.16 - a) Adsorption process of PRD with catalyst 3 at room temperature (20°C) after 3 minutes of mixing; b) Catalyst powder in A) fresh form and B) recycled form

3.2.2.6 Effect of different type of catalyst

Different catalysts such as 1, 2 and 3 with different Ag metal loadings were used for the reduction of phenol red where the influence of metal loadings on the rate of reaction were examined. As shown in Figure 3.17A, the rate of reduction rection steadily increased with the Ag metal loading on the cross-linked chitosan support. These observations are in agreement with the studies such as powder XRD and SEM-EDAX analysis, regarding the characterization of catalysts with different metal loadings. Further, the cross-linked chitosan showed lower activity compared to its Ag metal containing analogues and, in this case, $NaBH_4$ possibly contributed mainly to the reduction process. The Ag metal is therefore required for the reduction of the PRD since it is involved in the activation of H_2 obtained after the degradation of $NaBH_4$, which is further confirmation of previous research addressing the influence of catalyst quantity.

3.2.2.7 Reusability of catalyst

As with PNA, the reusability of catalyst 3 was examined in this dye reduction process. The Ag/chitosan catalyst 3 with 6.7 wt.% Ag metal loading was used for the recyclability study in case of reduction of PRD reduction process. The recyclability of the catalyst was carried out for 5 times. As shown in Figure 3.17B, the activity of the catalyst did not significantly decrease during the recycle study and the catalyst showed identical activities during all the recycle steps. It was observed a lower activity only between the use of fresh catalyst and all the recycling steps, since after 3, 6 and 9 minutes, the conversion achieved with recycled catalyst was lower compared to the fresh one. On the other hand, the time required to get a complete reduction of the dye did not change.

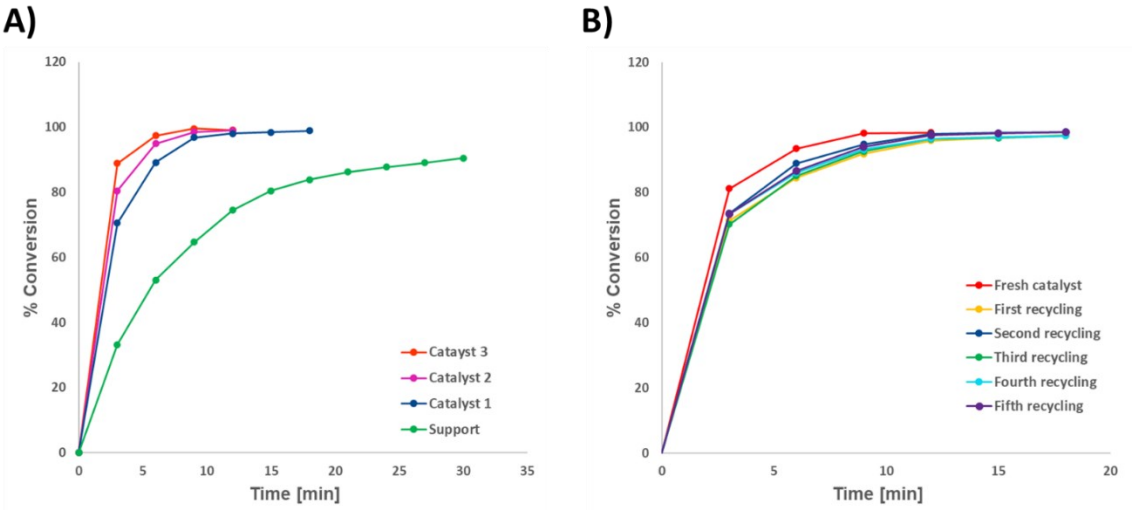

Figure 3.17 - Reduction of 2 mL of PRD solution 0.001 M at 20°C with 2.5 mg mL^{-1} of $NaBH_4$ and (A) 3 mg mL^{-1} of support and different type of catalysts and (B) 3 mg mL^{-1} of fresh and recycled catalyst 3

3.2.2.8 Evaluation of intrinsic uncertainty of laboratory measurements

Figure 3.17B shows that the conversion curves with respect to time for the PRD with new catalyst and recycled catalysts are equal. For this reason, it is reasonable to suppose that the intrinsic uncertainty of experimental measurements is the only factor affecting the variability of data. Therefore, as for the PNA, it is assumed that the data contained in Figure 3.17B are replications of the same measurements, which allows to quantify the experimental variability in terms of variance and standard deviation. These two parameters were calculated according to Equations 3.1 and 3.2, using the experimental observations of % conversion and concentration over time in the case of recycled catalysts. The corresponding results are displayed in Table 3.2.

***Table 3.2** - Variance and standard deviation values computed for the experimental tests of % conversion and concentration of PRD reduction with recycled catalysts considering 3-minute measurements*

	σ^2	σ
% Conversion	12	3.5
Concentration [mol/L]	$1.4 \cdot 10^{-9}$	$3.7 \cdot 10^{-5}$

3.2.3 Adsorption of phenol red dye

3.2.3.1 Adsorption of PRD on the catalyst followed by reduction

As it was previously observed in the analysis on PRD reduction with different concentration of

catalyst, in case of 3 mg mL^{-1} of catalyst 3 and 2.5 mg mL^{-1} of $NaBH_4$ at room temperature, complete reduction of the dye occurred in 12 minutes and the reaction mixture was further discoloured (Figure 3.18A). However, in the absence of $NaBH_4$, the reaction mixture become colourless in 6 minutes and the catalyst with violet colour on its surface was obtained (Figure 3.16). Figure 3.18B shows UV-spectra adsorption of PRD on Ag/CH catalyst 3, where it was observed that starting from the neutral PRD solution, the peak with λ_{max} value of 436 nm also decreased. According to Kwok *et al*. work (2014), chitosan surface is sensitive to the pH of the solution in which it is suspended where the adsorption of the arsenate ions effectively occurred in a solution with acidic pH range (below pH 7) while as the pH value increased above its neutral value, the rate of adsorption steadily decreased and the rate of desorption of the adsorbed species increased. This author also described the adsorption-desorption phenomenon of the arsenate ions in terms of point of zero charge (pHpzc) and surface charge density of the chitosan surface measured by potentiometric titration method. The pHpzc values of the studied chitosan particles were observed around 8, where above this value the surface became negatively charged. Besides that, the surface charged densities measurements also represented that the isoelectric point value was observed at 6.38, where the surface charge of the chitosan surface below this value was found positively charged. In other words, in the acidic range, the amine group in chitosan remined positively charged which allowed for the effective adsorption of the arsenate anion until neutral pH of the solution. Wang *et al*. (2008) also show equivalent observation in case of adsorption of fulvic acid over chitosan surface, where the point of zero charge study shows that the adsorption capacity of the adsorbent was high below pH 9 while it further decreased substantially over this value due to reverse of the charges of the surface from positive to negative. Wahab and Hussain (2016) studied the photodegradation of the PRD over nanocrystalline titanium oxide (TiO_2) particles where it was observed that since the TiO_2 surface remined positively charged under acidic conditions (below pH 6.5), the rate of degradation of the dye was increased and vice versa in case of alkaline medium. Further, the author presumed that under acidic to neutral pH conditions, the PRD also remained in the zwitterionic form or structure with negatively charged sulfate group which possesses an electrostatic attraction towards positively charged surface in a similar pH range (Figure 3.14). Ma *et al.* (2019) also applied chitosan as an adsorbent material for the adsorption of Congo red and methylene blue dye where the process was studied at dye solution under pH 6.5. Synthesized Ag/CH catalyst was treated with glutaraldehyde, and imine bonds were produced

instead of amine bonds of neat chitosan. Therefore, adsorption of PRD happened because these functional groups with nitrogen atom can have a behaviour similar to neat chitosan and adsorbs dye in acidic to neutral pH range.

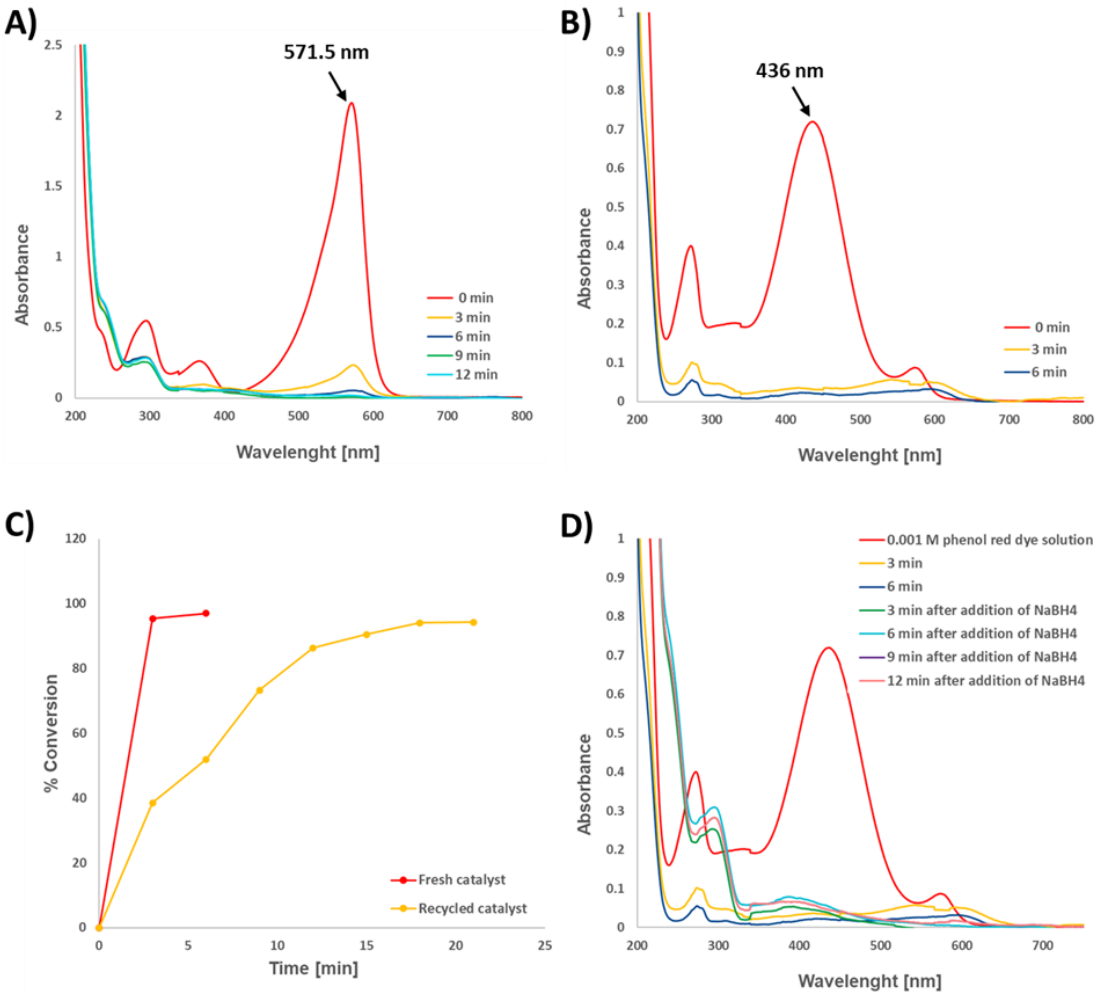

Figure 3.18 - UV-spectra of PRD reduction with 3 mg mL^{-1} catalyst 3, 2.5 mg mL^{-1} $NaBH_4$ at 20°C; (B) UV-spectra of adsorption of PRD on catalyst 3; (C) comparison between adsorption with fresh and recycled catalyst 3 at 20°C; (D) UV-spectra of adsorption followed by reduction of PRD with 3 mg mL^{-1} of Ag/CH catalyst 3 and 2.5 mg mL^{-1} of $NaBH_4$ at 20°C

The catalyst after the adsorption of dye was recovered and further again mixed with fresh PRD solution. As shown in Figure 3.18C, slow adsorption of the dye occurred on the recycled catalyst compared to fresh catalyst. Hence, these experiments illustrate that the besides reduction, the catalyst is capable to do the adsorption of the dye efficiently. Further, after adsorption of PRD over the catalyst surface, $NaBH_4$ was added to the reaction mixture, and it was observed that reaction mixture turned to fuchsia while it further discoloured in 15 minutes (Figure 3.18D).

3.2.3.2 Adsorption of PRD on the cross-linked chitosan followed by reduction

After confirmation of adsorption of dye on the catalysts, the cross-linked chitosan was also further examined in a similar adsorption process. Cross-linked chitosan also showed the high adsorption ability for the PRD over its surface and absorbance was decreased significantly in 6 minutes of processing time (Figure 3.19). Similar to the catalyst, the support was also able to perform adsorption of PRD under identical experimental conditions. Hence, this control experiment depicts that the adsorption of the dye is not limited to have Ag metal loaded on the catalyst surface and, as previously described, the positively charged surface of chitosan in acidic to neutral pH range can adsorb the dye efficiently.

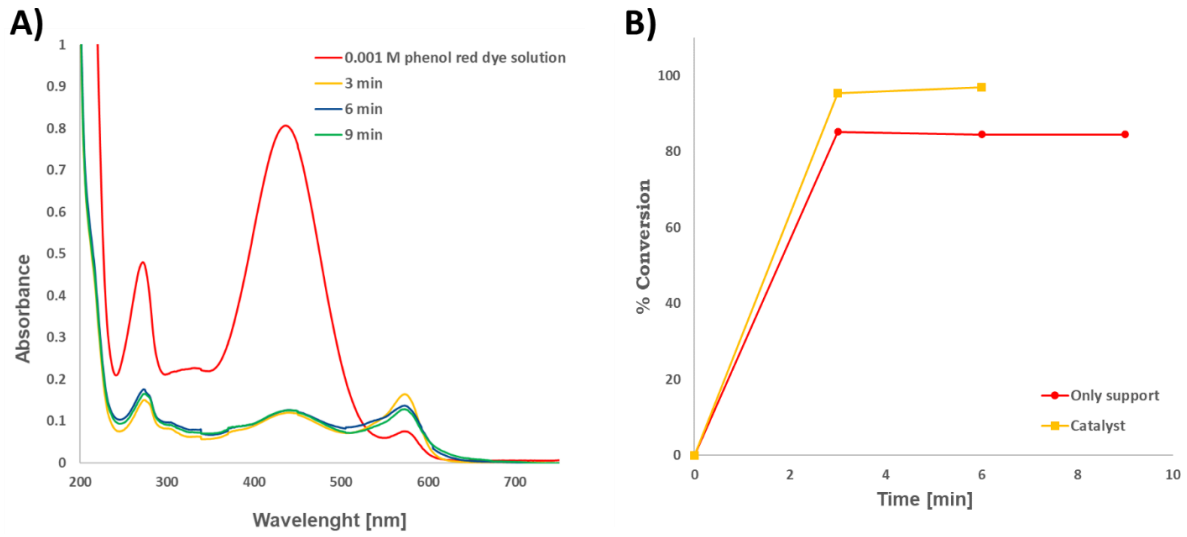

Figure 3.19 - A) Comparison between adsorption on cross-linked chitosan without Ag loading and adsorption on the catalyst 3. B) Adsorption and reduction of PRD with catalyst 3

After adsorption on the cross-linked chitosan, $NaBH_4$ was added to the reaction mixture to evaluate its reduction ability. The pH of the reaction mixture became alkaline, since $NaBH_4$ released NaOH, therefore the dye desorbed from the chitosan surface generating a fuchsia colour. In alkaline condition charges over the support and PRD become negative, such that adsorption is not possible, and dye desorbs instantaneously. The reduction of the dye with the combination of cross-linked chitosan + $NaBH_4$ proceeds slower than the case in which the combination Ag/CH + $NaBH_4$ was used. Even in the case in which the lower amount of Ag/CH catalyst 3 was used (0.5 mg mL^{-1}), the reaction rate was faster, because complete reduction was obtained in 21 minutes (Figure 3.15A), while with cross-linked chitosan complete reduction

was not achieved even after 30 minutes, because only 79% of conversion was obtained (Figure 3.20). Reduction of dye with cross-linked chitosan support occurred mainly because of the presence of $NaBH_4$, since it was demonstrated that the reducing agent was able to degrade the dye even without catalyst, but with a slower reaction rate (Figure 3.15A). These experiments demonstrate that PRD is able to adsorbs on cross-linked chitosan and Ag/CH catalyst with a comparable rate. On the other hand, reduction of the dye is efficient only in the case in which catalysts with silver nanoparticles is used.

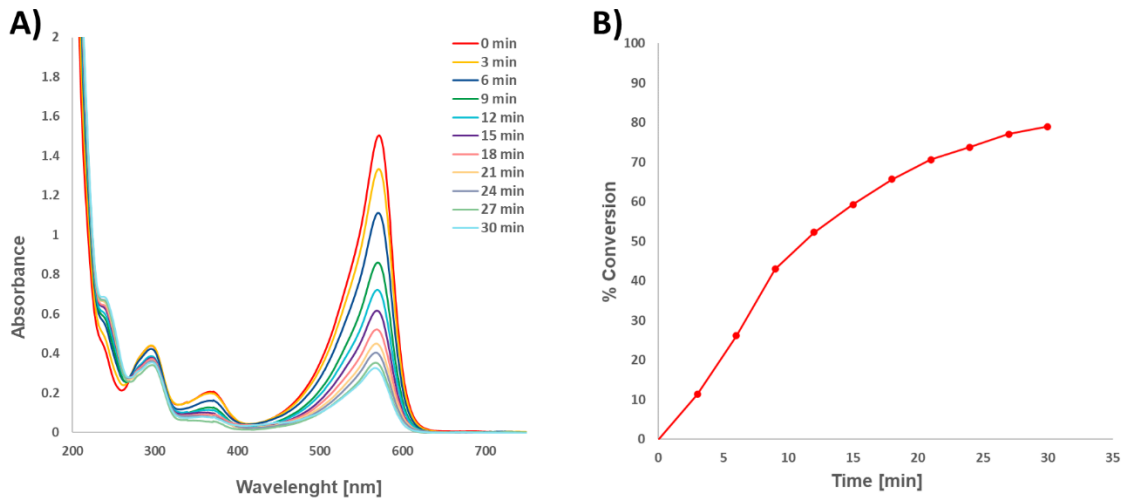

Figure 3.20 - (A) Adsorption followed by reduction of PRD with 3 mg mL^{-1} of cross-linked chitosan and 2.5 mg mL^{-1} of $NaBH_4$ at 20°C; (B) Percentage of conversion of PRD in the adsorption process followed by reduction with cross-linked chitosan support

3.2.4 Reduction and adsorption of PRD in an alkaline solution (pink colored solution)

All the previous experiments regarding the reduction and adsorption study were performed with fresh PRD solution while the pH of the solution was below or near to its neutral value. Now, the dark fuchsia colored solution obtained after preparation of 0.001 M solution of dye in 0.1N solution was further used for the reduction and adsorption process. In other words, the rate of adsorption as well as reduction were examined under initial pH of the solutions. After addition of catalyst 3 (i.e. with 6.7 wt.% Ag) in the alkaline solution of PRD, the rate of adsorption significantly decreased and a considerable amount of dye remained in the solution. As shown in Figure 3.21A, the PRD under neutral pH was completely adsorbed in 6 minutes while merely 20% of the dye was adsorbed in 21 minutes when alkaline solutions were applied. Similar to

the adsorption process, the reduction ability of the dye was examined in alkaline solution of PRD whereupon both catalysts 3 and $NaBH_4$ were mixed with alkaline solution and the obtained results are shown in Figure 3.21B. The rate of reduction of dye decreased in an alkaline solution and slow reduction was observed compared to the red-orange colored solution. Hence, these controlled experiments confirm that pH of the PRD in aqueous solutions is important in case of both adsorption and reduction. Hence, as described previously, the alkaline conditions are not favorable to the adsorption of the dye since under alkaline pH, both the chitosan surface as well as dye converted to negatively charged entities and did not allow efficient adsorption (Kwok *et al*., 2014; Wang *et al*., 2008; Wahab and Hussain, 2016; Ma *et al.*, 2019). On the other hand, solutions with pH near to neutral were allowing efficient processing of the dye since the chitosan surface remained positively charged and allowed adsorption and the subsequent reduction of the dye.

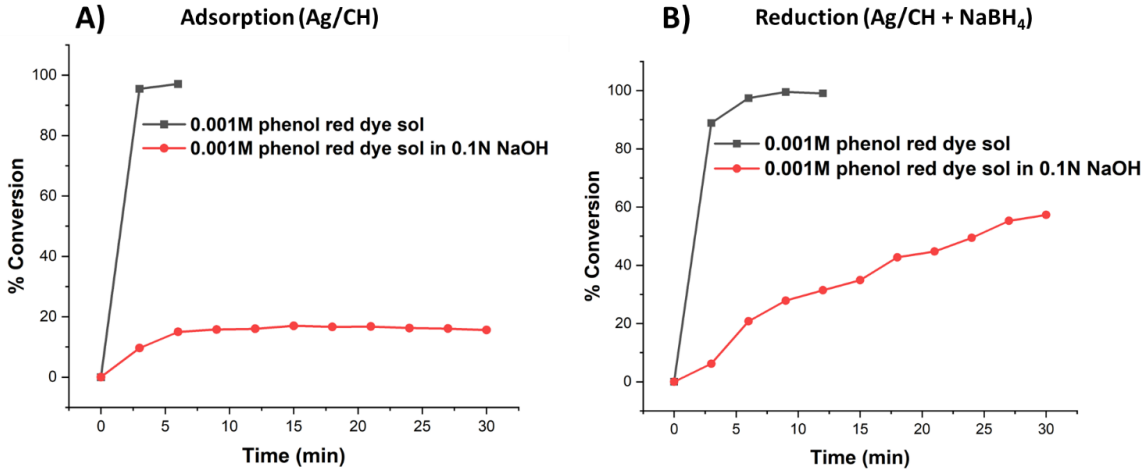

Figure 3.21 - (A) Adsorption with catalyst 3 of neutral and alkaline PRD solution; (B) Reduction with catalyst 3 of neutral and alkaline PRD solution by using 2.5 mg·mL^{-1} of $NaBH_4$

3.2.5 Proposed mechanism of reaction for PRD reduction

Considering the study regarding the adsorption and reduction process of PRD solution, under both neutral and alkaline condition, the mechanism for the reduction was proposed and is shown in Figure 3.22. After addition of the catalyst and $NaBH_4$ in the red-orange solution of PRD solution, the dye got adsorbed over the catalysts support. Simultaneously, $NaBH_4$ decomposed

slowly in aqueous medium and released H_2 and NaOH. Ag metal over the catalyst further activated the released H_2 and reduced adsorbed dye simultaneously. The pH of the solution increased slowly due to release of NaOH and it further lowered the reduction rate of dye due to slow desorption of dye from the catalysts surface. Hence, in this case, chitosan support did not only allow for the adsorption of the dye but also stabilized the Ag metal to further activate H_2 and reduce the dye, accordingly.

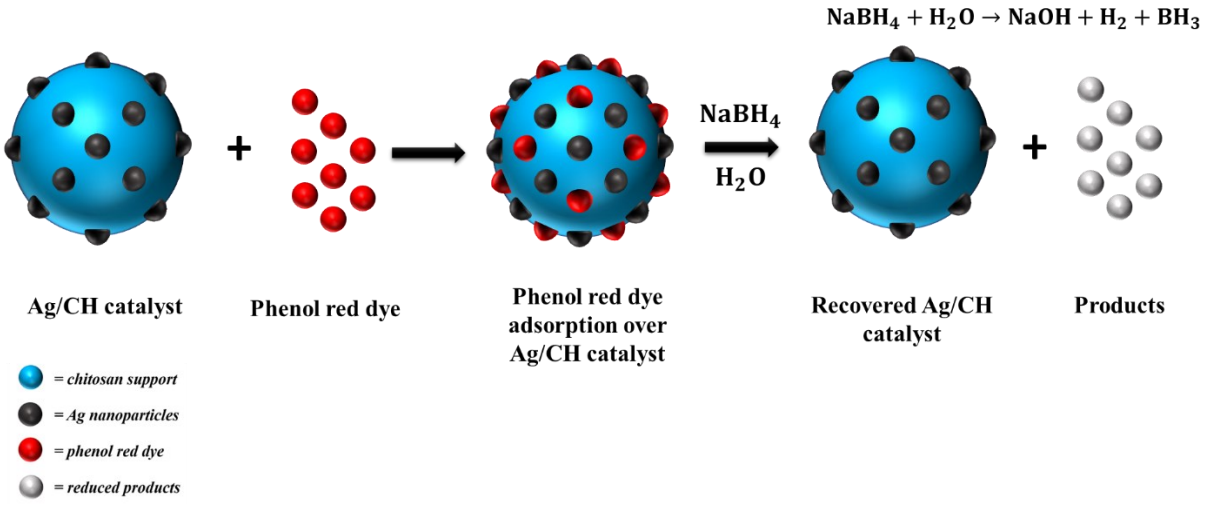

Figure 3.22 - Proposed mechanism of PRD reduction with $NaBH_4$ and Ag/CH catalyst

3.2.6 Suggestions and perspectives

The experiments analyzed in this chapter demonstrate that the Ag/CH catalyst degrades the two organic dyes under study very effectively and quickly. Additionally, in the case of PRD, the catalyst has the ability to absorb the organic compound, so the use of the reducing agent is not required. To further evaluate the catalyst and develop its application, some research could be done. Additional studies could be performed to determine whether the catalyst may be used to treat water contaminated with organic dyes and other similar compounds. Other experiments could be conducted to understand whether the progress of both reactions depends on the reagent/catalyst concentration ratio. Some studies could be done to determine whether PRD absorption on the catalyst is more convenient than reduction with $NaBH_4$, as the use of this reducing reagent should be carefully considered to determine whether it releases any potentially harmful substances into the reaction environment. On this regard, the use of gaseous H_2 was tried at the beginning of the experiments, to evaluate the substitution of $NaBH_4$, but no good

result was obtained. Furthermore, an extra study could be performed to understand the structure of the final product of the phenol red dye reduction.

Chapter 4
Kinetic study

A kinetic study is the investigation of the reactions rates and mechanisms of chemical reactions. The procedure starts from experimental data, like $\underline{\mathrm{N}}^{\mathrm{exp}}, \underline{\dot{\mathrm{N}}}^{\mathrm{exp}}, \underline{\mathrm{c}}^{\mathrm{exp}}$, from which it is possible to speculate about the kinetics, namely to predict the mechanism $\underline{\underline{\nu}}$ and the rates $\underline{\mathrm{R}}$. In literature, database about the rates of reactions are available, including examples of expressions and the parameters utilized in such expressions. On the other hand, this information is not enough, because they are reaction specific and not complete. Furthermore, this information is not very reliable because it is impossible to know precisely the mechanism. For example, an interaction between two species like A+B can give rise to different products, like C+D, but new intermediates are continuously formed along reaction steps. Another important concept of kinetics is that in literature there is a wide variety of chemistry. The conclusion is that kinetics can only be inspired by literature, because it can give a suggestion of a starting point, but usually an adjustment is needed. Thus, kinetics study is a fundamental tool of chemical reaction engineering. Experiments are the most used and reliable approach to identify kinetics, because from them the mechanism and the corresponding expression of the reaction rate can be obtained. Experimental data are connected to reaction rates and mechanism through the material balances (MBs). The behaviour of the systems and species is available $\left(\underline{\mathrm{c}}^{\mathrm{exp}}\right)$, and through the MBs the mechanism can be identified. Since MBs are the key, different reactors are characterized by different approaches. Considering the ideal reactors, two different approaches are used:

1. Batch/PFR at $\hat{\rho} = const$:

$$\frac{d\underline{\underline{c}}}{d\tau} = \underline{\underline{r}}(\underline{\underline{\nu}}, \underline{R}) \tag{4.1}$$

2. CSTR at $\hat{\rho} = const$:

$$\frac{\Delta\underline{\underline{c}}}{\vartheta} = \underline{\underline{r}}(\underline{\underline{\nu}}, \underline{R}) \tag{4.2}$$

In this thesis, a kinetic study was carried out for both the reduction. Both the reactants have been processed in a reacting system that can be treated as a batch reactor.

4.1 Kinetic study for a batch reactor

4.1.1 Differential approach

For a batch reactor, perfectly mixed conditions are assumed, and the procedure starts with the identification of the concentration of the reactant or the products at time zero. Considering the material balances referred to the reactant i, the concentration at the initial time $t = t_0 = 0$ is identified as c_i^0. At a generic time instant t_1, a sample of liquid is taken and analyzed, and the concentration of the reactant is measured. MBs can be approximated as:

$$\left.\frac{\Delta c_i}{\Delta t}\right|_1 = \frac{c_i|_1 - c_i^0}{t_1 - t_0} \cong \frac{dc_i}{dt} = r_i = \nu k c_i^{\alpha} \tag{4.3}$$

In the expression 4.3, it is possible to assume the stoichiometric coefficient $\nu = -1$ and the reaction rate can be expressed as $R = kc_i^{\alpha}$, therefore the rate of consumption of i is given by $r = -kc_i^{\alpha}$. Therefore, it was obtained:

$$\frac{dc_i}{dt} = -k\bar{c}_i^{\alpha} \tag{4.4}$$

where $\bar{c}_i$ is an average concentration between the one measured at the initial time instant t_0 and the one measured at the generic time instant t_1:

$$\frac{c_i^0 + c_i|_1}{2} \tag{4.5}$$

Another measurement at the next time instant t_2 can be done, such that a second average concentration can be obtained:

$$\frac{c_i|_1 + c_i|_2}{2} \tag{4.6}$$

Two equations are obtained, and, since they are coupled, they can be solved with respect to the

two unknowns k and α:

$$\begin{cases} \left.\frac{\Delta c_i}{\Delta t}\right|_1 = \frac{c_i|_1 - c_i^0}{t_1 - t_0} \cong \frac{dc_i}{dt} = -kc_i^\alpha \\ \left.\frac{\Delta c_A}{\Delta t}\right|_2 = \frac{c_A|_2 - c_A|}{t_2 - t_1} \cong \frac{dc_A}{dt} = -kc_A^\alpha \end{cases} \Rightarrow \begin{cases} \frac{dc_i}{dt} = -k\left(\frac{c_i^0 + c_i|_1}{2}\right)^\alpha \\ \frac{dc_i}{dt} = -k\left(\frac{c_i|_1 + c_i|_2}{2}\right)^\alpha \end{cases} \quad (4.7)$$

With this approach, the variation of concentration is approximated to a linear law; to get a better approximation of the real behaviour of concentration with respect to time, it is necessary to choose very small Δt or Δc_i such that the two points are close one to each other and the predictions of variation in concentration are better. With this technique, the slope of the curve about concentration over the time is identified. Once it is known, the initial slope is able provide information about the initial rates since it is defined as the rate of production/consumption. In this way, from the initial slope the kinetic parameters *k* and *α* are retrieved. The results are very uncertain because of uncertainty of measurement and small Δt. Uncertainty of measurements is an important issue of kinetic study since it can make difficult to determine the true rate of the reaction or the reliable concentrations of the reactants and products. As a results, the conclusion of the study may be impacted, and the kinetic parameters may be incorrect. The method just described is called differential, because small differential intervals are used to speculate about the slope.

4.1.2 Integral approach

Another approach is the integral method. It is developed in opposition to the differential method because it predicts all the behaviour through the integration of the material balances, while the differential method tries to identify the local slope. Integral approach is applied especially for PFR and batch reactor. The goal is to solve MBs:

$$\frac{dc_i}{dt} = r_i \quad (4.8)$$

The analytical solution of the balance equation 4.8 is $c_i^{th}(r_i)$, assuming a mechanism and a

reaction rate. The procedure can be summarized in different steps. First, experimental concentration of the reactant or products over the time must be collected and plot. Depending on their shape, some hypotheses are made, and a mechanism $\underline{\nu}$ and a reaction rate $\underline{R}$ can be suggested. The reaction rate is a function of the concentrations $\underline{c}$ and parameters $\underline{\beta}$ that are present in the model. For example, if it is assumed a reaction rate like $R = kc_i^{\alpha}$, the vector of the parameters is $\underline{\beta} = (k, \alpha)$. The next step is the setup of the MBs, which are solved with respect to the parameters $\underline{\beta}$. A first guess on the values of the parameters is introduced and then $c_i^{th}(t)$ can be obtained solving the material balance on the species i. Assuming a reactant, MB is:

$$\begin{cases} \dfrac{dc_i}{dt} = r_i = \nu_i R = -kc_i^{\alpha} \\ c_i(0) = c_i^0 \end{cases} \tag{4.9}$$

Experimental value $c_i^{exp}(t)$ and the theoretical prediction $c_i^{th}(t)$ obtained with the assumed mechanism and rate are compared. If the theoretical values do not fit the experimental one, the model or the mechanism needs to be adjusted, or the value of the parameters $\underline{\beta}$ need to be changed, and then the procedure needs to be re-started again. The best $\underline{\beta}$ is the one that is close to the average of all the experimental data. To understand if the $\underline{\beta}$ used is the correct one, a distance is introduced, which is defined as the absolute value of the difference between the experimental and theoretical concentration evaluated at the same time (Equation 4.10).

$$D = \left| c_i^{exp}(t) - c_i^{th}(t) \right| \tag{4.10}$$

The higher the number of experimental measurements, the higher the number of distances that can be computed. D is a vector, characterized by all the distances between the experimental and theoretical concentration. Therefore, a norm is used to combine all the elements of the vector D:

$$D = \|D_n\| \tag{4.11}$$

In the equation 4.11, n indicates the number of experiments $n = 1..N_{exp}$. D varies with the parameters $\underline{\beta}$ used in the model, and the lower is D the better is the model. Thus, the values of

the parameters need to be chosen such that the distance between the model and data is minimized:

$$\min_{\underline{\beta}} D\left(\underline{\beta}\right) \tag{4.12}$$

A minimization routine needs to be used. This procedure can be implemented in MATLAB, where the minimization routine can be the function `fminsearch`. `fminsearch` searches for the minimum of a problem specified by $\min_x f(x)$, where f(x) is a function that returns a scalar, and x is a vector or a matrix. In general, it is used in an expression like `[x,fval] = fminsearch(fun,x0,options)`: the research starts at the point `x0` and attempts to find a local minimum x of the function described in `fun`. When the expression `options` is present, `fminsearch` minimizes the function with the optimization options specified in the structure `options`. `Optimset` is used to set these options.

In this work, kinetic study was applied to both the reactions and an integral approach was used and implemented in MATLAB with the minimization routine `fminsearch`. The procedure is the same for both the reactions. `[k,fval] = fminsearch(@err,k0,opt,texp,Cexp)` is the expression used in MATLAB for the kinetic study to find the minimum of the function `err`, which computes the norm of the distance between the experimental and theoretical concentration evaluated at the same time (Equation 4.10). `k0` is the vector of the parameters $\underline{\beta}$ of the assumed reaction rate and represents the starting point for the research of the minimum of the function `err`. `Ode15s` is the function used in MATLAB to solve the MBs.

4.2 Kinetic study for p-nitroaniline

Reduction of PNA with $NaBH_4$ and Ag/CH gives rise to the formation of PPD (Figure 4.1). The kinetic study of this reduction was carried out following the procedure explained in the paragraph 4.1.2 and introducing some assumptions. The starting aqueous solution of PNA 0.001 M was assumed to be perfectly homogeneous, without having some remaining granules in solid form. The reaction proceeds with the adding of $NaBH_4$ in powder form and Ag/CH in the PNA solution, therefore it was assumed that $NABH_4$ dissolved completely and instantaneously. Furthermore, it was also assumed that by-products were not formed, but PPD was the only product obtained from the reacting process. The kinetic study was performed considering the

decrease in concentration of the reactant, since the monitoring of the progress of reaction with the UV-spectrophotometer was done measuring the concertation over the time of PNA. The experiment was such that 2 mL of 0.001 M PNA reacted with 2.5 mg mL^{-1} of $NaBH_4$ and 0.5 mg mL^{-1} of Ag/CH catalyst 3 at constant stirring (500 rpm). It is important to consider that a lot of volume of the reacting system was removed during the measurement of concentration, because 0.1 mL were taken for each test and at the end of the reaction, it was measured a reduction in volume of 20-40%, depending on the number of tests performed. This could be a problem, but only if a change of the ratio liquid/catalyst occurred. It was assumed that both liquid and catalyst were sampled uniformly, i.e. with the same ratio liquid-to-catalyst of the reactor, because it is very difficult to remove only liquid without catalyst. Therefore, the change in volume of the reacting system does not alternate the reactions, because the ratio liquid/catalyst remains the same.

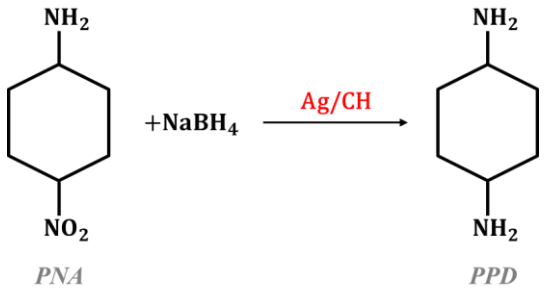

Figure 4.1 - Reaction scheme of PNA reduction with Ag/CH and $NaBH_4$

The reaction between PNA and $NaBH_4$ took place in the liquid, after their adsorption on the Ag/CH surface. It was assumed that the adsorption was extremely fast, and it can be neglected. Therefore, the reaction rate was proposed as:

$$R = kc_{PNA}^{\alpha_1} c_{NaBH_4}^{\alpha_2} \tag{4.13}$$

k is the kinetic constant, c_{PNA} and c_{NaBH_4} are the concentration of PNA and sodium borohydride, respectively, and α_1 and α_2 are the exponents of the concentration of the two reactants. All the experiments were carried out with an excess of $NaBH_4$, because according to the stoichiometry 1 mole of PNA requires 1 mole of $NaBH_4$, and in the tests the moles of hydrogen source used are two orders of magnitude higher than the one of PNA. Thus, to simplify the kinetic study it was assumed that $NaBH_4$ concentration is constant and included in

the kinetic constant, and the reaction rate becomes:

$$R = kc_{PNA}^{\alpha} \tag{4.14}$$

According to the previous assumptions on change in volume, the corresponding material balance for the PNA reduction is shown in Equation 4.15.

$$\frac{dc_{PNA}}{dt} = r_{PNA} = \nu_{PNA} R = -R \tag{4.15}$$

4.2.1 First-order reaction for PNA reduction

From Figure 4.2, in which experimental concentrations of PNA are plotted with respect to the time at 20°C, it seemed reasonable to assume a first-order reaction, that means $\alpha = 1$.

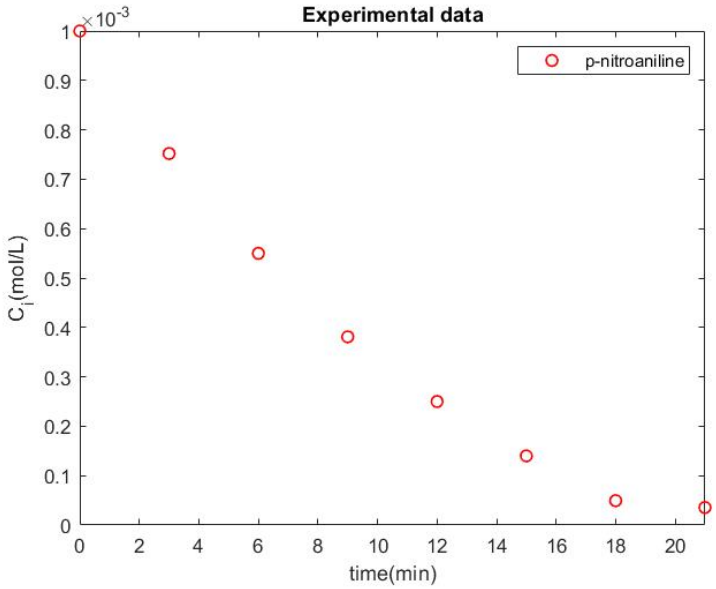

Figure 4.2 - Experimental concentration vs. time of PNA during catalytic reduction with51 mg of $NaBH_4$ and 0.5 mg mL^{-1} of Ag/CH catalyst 3

In this case, the material balance becomes:

$$\begin{cases} \dfrac{dc_{PNA}}{dt} = r_{PNA} = -kc_{PNA} \\ c_{PNA}(t=0) = c_{PNA}^{0} \end{cases} \tag{4.16}$$

And the corresponding analytical solution is:

$$c_{PNA}^{th} = c_{PNA}^{0} \exp(-kt) \tag{4.17}$$

The method used for the kinetic study was the integral approach. The material balance was implemented in MATLAB, and an initial guess of the parameters was given. Since it was assumed a first-order kinetics, the vector of the parameters $\underline{\beta}$ become a scalar made of an initial value of the kinetic constant k.

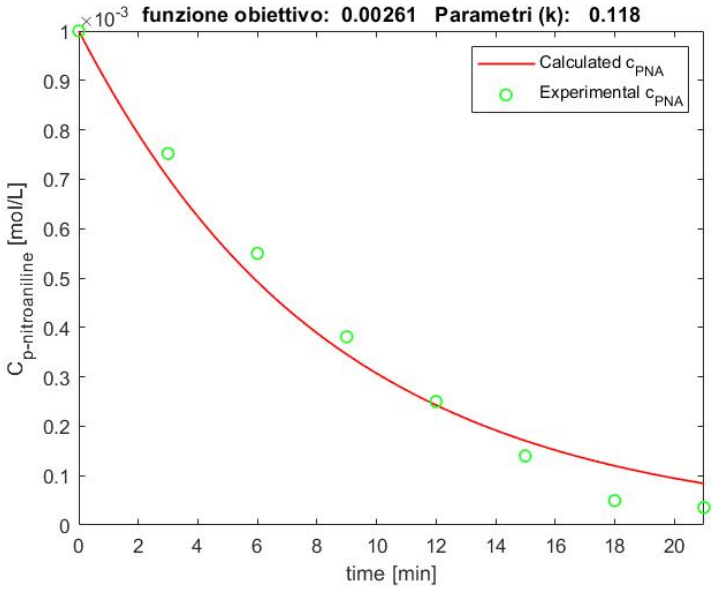

Figure 4.3 - Predictions vs experimental data along the reaction time of PNA reduction with a first-order kinetic

The initial guess and the final results for k are reported in Table 4.1. Figure 4.3 shows the comparison between $c_{PNA}^{exp}(t)$ and $c_{PNA}^{th}(t)$ with respect to the reaction time. It was observed that the calculated curve does not perfectly fit the experimental data, thus the model used to describe the reaction rate needs to be modified. A first-order reaction for this process is not enough, and it is necessary to move to a reaction rate with $\alpha \neq 1$.

***Table 4.1** - Initial guess and final value of the kinetic constant for PNA reduction*

	k [s^{-1}]
Initial guess	0.02
Final value	0.118

4.2.2 Introduction of α in the kinetic model for PNA

The material balance was re-written in the following form:

$$\begin{cases} \dfrac{dc_{PNA}}{dt} = r_{PNA} = -kc_{PNA}^{\alpha} \\ c_{PNA}(t=0) = c_{PNA}^{0} \end{cases} \tag{4.18}$$

The difference with respect to a first-order reaction is the presence of the exponent α. This means that two initial values need to be assigned to the parameters $\underline{\beta} = (k, \alpha)$ (Table 4.2). The procedure is the same, and the same function were used in MATLAB to solve the material balance. With the introduction of $\alpha \neq 1$, the fitting of the experimental data becomes better. On the other hand, it can be observed that the concentration at 18 minutes is far from the calculated curve (Figure 4.4).

Table 4.2 *- Initial guess and final value of parameters for p-nitroaniline reduction*

	k	**α**
Initial guess	0.02 $mol^{0.3}\,L^{-0.3}\,s^{-1}$	0.7 [-]
Final value	0.0183 $mol^{0.25}\,L^{-0.25}\,s^{-1}$	0.75 [-]

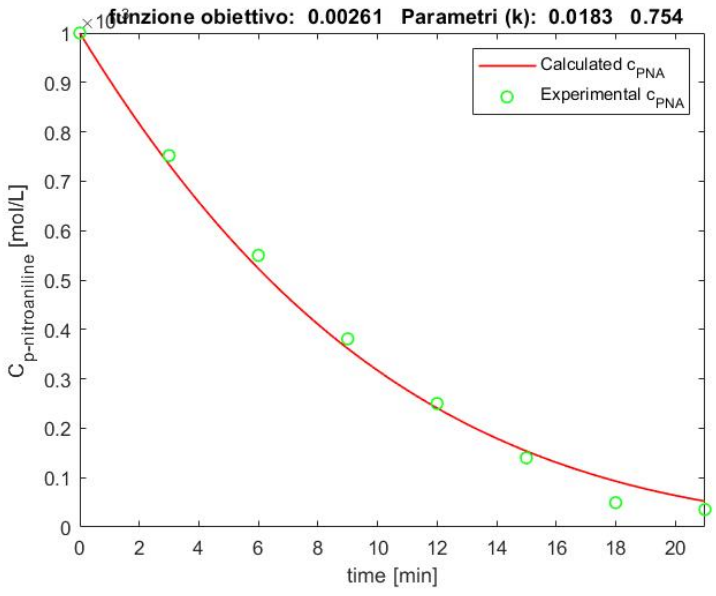

Figure 4.4 - Predictions vs experimental data along the reaction time of PNA reduction with a non-elementary reaction

Predictions are compared with respect to the experimental values in the parity plot, including bands of relative errors of ±10% (Figure 4.5). The comparison between the two parity plots

shows a better situation in the case of non-elementary reaction, with $\alpha < 1$, because all the points are within the bands of relative errors of ±10%, except for the last two. In the case of a first-order reaction, the distribution of the data is more scattered, and more points are outside the bands of relative errors. A perfect match between experimental data and computed concentrations is impossible to achieve, especially for all the assumptions made, but the fitting providing the concentration profiles along the reaction time with $\alpha < 1$ is quite matching the experimental values, even if in some parts computations are not so accurate.

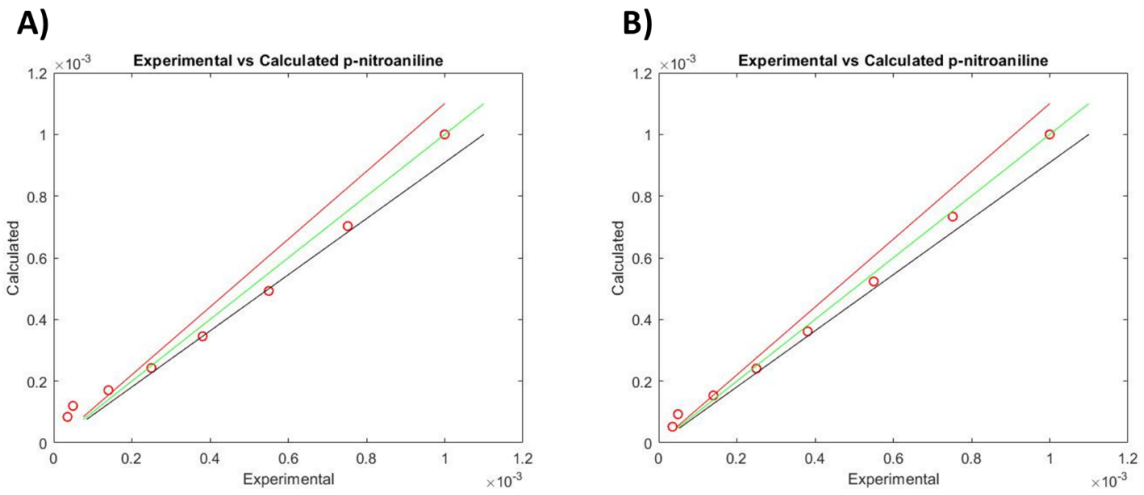

Figure 4.5 - Predictions vs experimental value of PNA reduction with bands of relative errors of ±10% of kinetic study assuming A) a first-order reaction and B) a non-elementary reaction

One of the objectives of a kinetic study is to find the pre-exponential factor and the activation energy of the reaction through the determination of the kinetic constant. To do that, it is necessary to have different kinetic constants at different temperatures. Therefore, the kinetic study needs to be performed also for the datasets at 25 and 30°C. Kinetic constants are functions of temperature, while alpha does not depend on temperature. Therefore, the calculations were implemented considering $\alpha = 0.75$. The procedure used for the kinetic study at the different temperature was exactly the same and the results are summarized in Table 4.3 and Figure 4.6.

Table 4.3 *- Final values of kinetic constant obtained through the kinetic study applied to experimental measurement at different temperature for PNA reduction assuming a non-elementary reaction*

	k [mol$^{0.25}$ L$^{-0.25}$ s^{-1}]	**α [-]**
20°C	0.0177	0.75
25°C	0.0274	0.75
30°C	0.0361	0.75

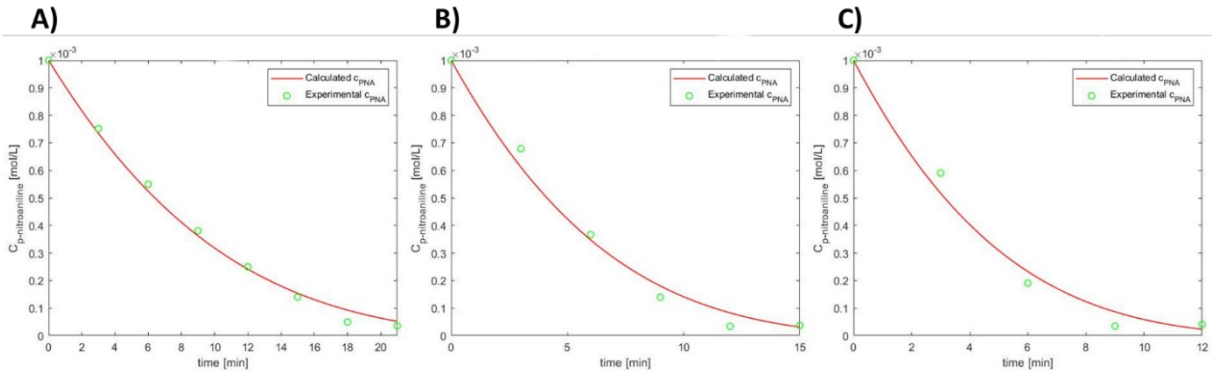

Figure 4.6 - Experimental concentration vs calculated concentration over reaction time of p-nitroaniline reduction assuming a non-elementary reaction with α = 0.75 for experimental measurements at A) 20°C, B) 25°C and C) 30°C

To assess the accuracy of the kinetic model used, error bars can be added in the Figure 4.6. This can be done by using the standard deviation determined in §3.2.1.7, so that error bars with an σ half-width are used. In this way, it is assumed that around each experimental measurement there is a normal distribution.

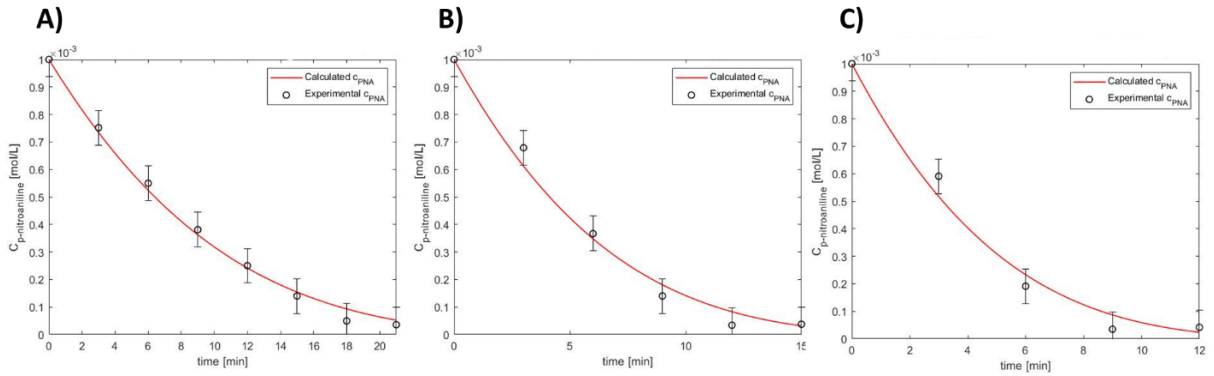

Figure 4.7 - Experimental concentration vs calculated concentration over reaction time with error bars of PNA reduction assuming a non-elementary reaction with α = 0.75 at A) 20°C, B) 25°C and C) 30°C

With the addition of the error bars, it is clear that the curve of the calculated concentration of PNA passes through them (Figure 4.7). It is correct that the calculated concentration curve does not pass through all experimental points since they are affected by experimental error, but if the kinetic model enters all bands, it is reasonable to assume that it describes well the kinetics of the reaction under study.

4.2.3 Calculation of activation energy and pre-exponential factor for PNA reduction

Activation energy and pre-exponential factor can be calculated using the Arrhenius equation, which relates the rate constant of a chemical reaction to temperature:

$$k = Aexp\left(-\frac{E_a}{R}\cdot\frac{1}{T}\right) \tag{4.19}$$

In Equation 4.19, A is the pre-exponential factor, E_a is the activation energy, R is the universal gas constant, and T is the absolute temperature in Kelvin. To determine A and E_a using this equation, three kinetic constants (k_1, k_2, k_3) previously determined (Table 4.3) at 20, 25 and 30°C were used. To obtain A and E_a, one common approach is to take the logarithm of Arrhenius equation:

$$\ln k = \ln A - \frac{E_a}{R}\cdot\frac{1}{T} \tag{4.20}$$

This equation can be associated to the expression of a straight line in the form $y = mx + q$, where $y = \ln k$, $q = \ln A$, $m = -E_a/R$ and $x = 1/T$.

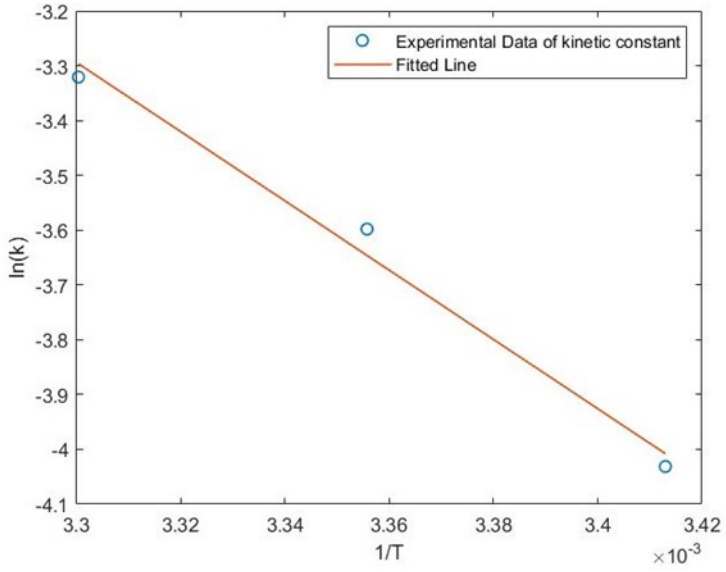

Figure 4.8 - Experimental values of k vs fitted line obtained with linear regression employing Arrhenius equation

A linear regression of the three kinetic constants at different temperature can be implemented in MATLAB, employing the function `polyfit` which is used to fit a polynomial curve to a set of data points (Figure 4.8). Using $R = 8.314\ J\ mol^{-1}K^{-1}$, it was obtained $E_a = 52509\ J\ mol^{-1}$ and $A = 4.18 \cdot 10^{7} mol^{0.25}\ L^{-0.25}\ s^{-1}$.

4.3 Kinetic study for phenol red dye reduction

The objective of PRD reduction is to remove it from wastewater, since it is considered as a harmful compound. Its reduction was performed with $NaBH_4$ and synthesized Ag/CH catalyst (Figure 4.9).

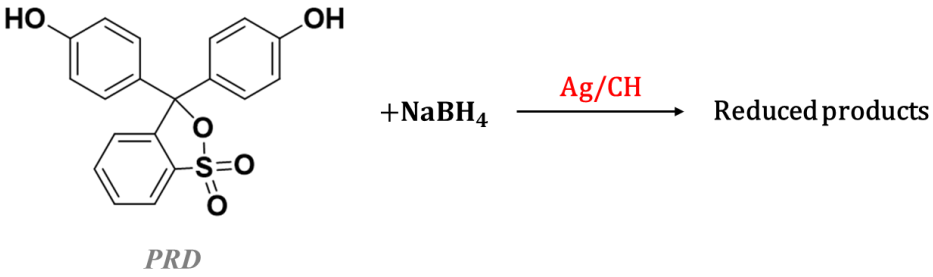

Figure 4.9 - Reaction scheme of phenol red reduction with Ag/CH catalyst and $NaBH_4$

The kinetic study was carried out with the same procedure applied to PNA, and with the same assumptions about homogeneity of starting PRD solution, dissolution of $NaBH_4$, formation of by-products, change in volume of the reacting system. Furthermore, PRD and $NaBH_4$ reacted in the liquid after adhering to the Ag/CH surface, but the adsorption can be ignored since it is very quick. $NaBH_4$ and PRD are in a stoichiometric ratio equal to 1:1, but in the experiments an excess of $NaBH_4$ was used since the difference in moles between the two reactants was one order of magnitude. As in the case of PNA, $NaBH_4$ can be included in the kinetic constant since it was used in excess during reactions. The corresponding reactions rate and material balances are reported in Equation 4.21 and 4.22, respectively.

$$R = k c_{PRD}^{\alpha} \tag{4.21}$$

$$\frac{dc_{PRD}}{dt} = r_{PRD} = \nu_{PRD} R = -R \tag{4.22}$$

The experiments conducted for the study are those where 2 mL of 0.001 M PRD reacted with

0.5 mg mL^{-1} of $NaBH_4$ and 3 mg mL^{-1} of Ag/CH catalyst 3 at constant stirring (500 rpm). Different temperatures were applied, in order to compute also the pre-exponential factor, and activation energy once the kinetic constants were obtained. Data at 20°C are shown in Figure 4.10A. It was observed that these data have a strange distribution, therefore a comparison with data at 30°C and 40°C was done (Figure 4.10B). It seems that some errors occurred during the measurement at 20°C, because they have a completely different behaviour with respect to the other two temperatures. Looking at the values after 3 minutes (Figure 4.10B), it was observed that the decrease in concentration at 20°C and 30°C is very similar, that is not so realistic considering the difference in temperature of 10°C. Therefore, the dataset at 20°C was not considered for the data fitting during the kinetic study.

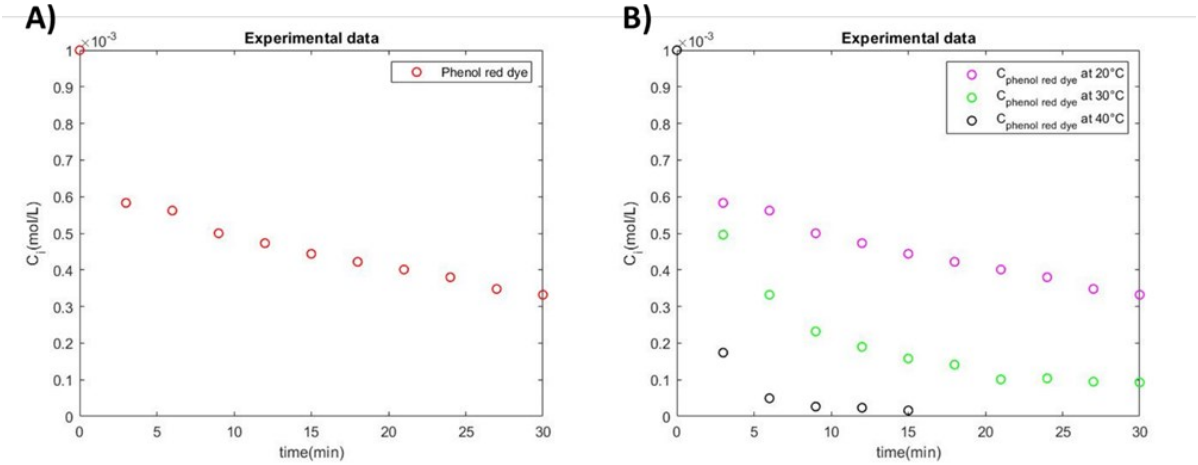

Figure 4.10 - (A) Experimental concentration vs. time of PRD during catalytic reduction with 0.5 mg mL^{-1} of $NaBH_4$ and 3 mg mL^{-1} of Ag/CH catalyst 3 at 20°C (B) comparison between experimental data of PRD reduction at 20°C, 30°C and 40°C

4.3.1 First-order reaction for PRD reduction

A first attempt with $\alpha = 1$ was done. The material balances become:

$$\begin{cases} \dfrac{dc_{PRD}}{dt} = r_{PRD} = -kc_{PRD} \\ c_{PRD}(t=0) = c_{PRD}^{0} \end{cases} \tag{4.23}$$

Results are reported in Table 4.4 and Figure 4.11.

***Table 4.4** - Initial guess and final value of kinetic constant k assuming first-order kinetic for PRD reduction*

	k at 30°C [s^{-1}]	k at 40°C [s^{-1}]
Initial guess	0.02	0.02
Final value	0.135	0.491

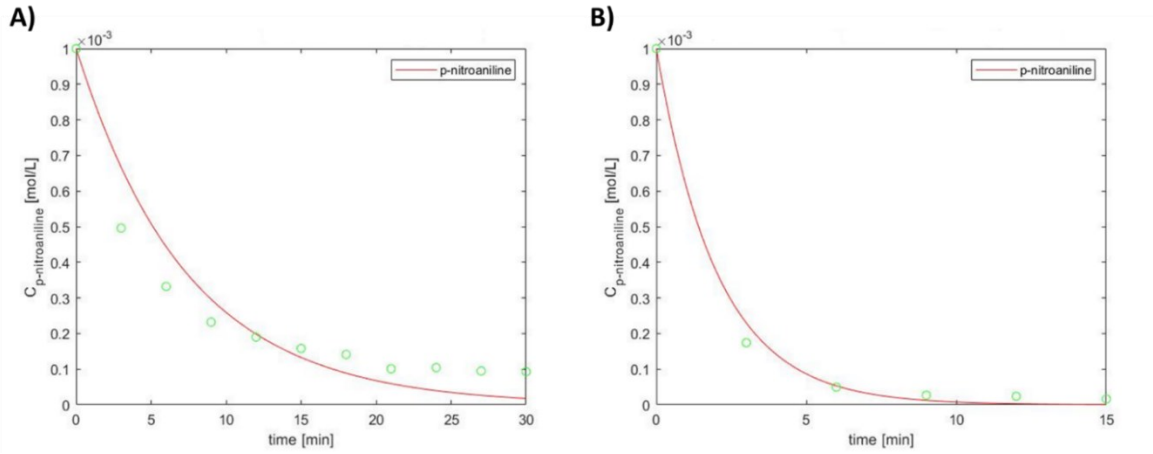

Figure 4.11 - Predictions vs experimental data along the reaction time of phenol red dye reduction with a first-order reaction at A) 30°C and B) 40°C

$c_{PRD}^{exp}(t)$ and $c_{PRD}^{th}(t)$ with respect to the reaction time are comparable in the case of data at 40°C, while at 30°C the experimental data are not properly fit by the curve. To get a better fitting of the data at 30°C, a modification of the kinetic model is needed, by introducing a non-elementary reaction, i.e. with $\alpha \neq 1$.

4.3.2 Introduction of α in the kinetic model for PRD

With the introduction of α, the reaction rate becomes $R = kc_{PRD}^{\alpha}$. The results of this study are shown in Table 4.5 and Figure 4.12, assuming an initial guess for the parameters equal to $\beta = (0.8, 0.8)$.

***Table 4.5** - Final values of parameters assuming a non-elementary reaction for PRD reduction*

	k	α
30°C	239 $mol^{-0.95}\,L^{0.95}s^{-1}$	1.95 [-]
40°C	14.9 $mol^{-0.41}\,L^{0.41}\cdot s^{-1}$	1.41 [-]

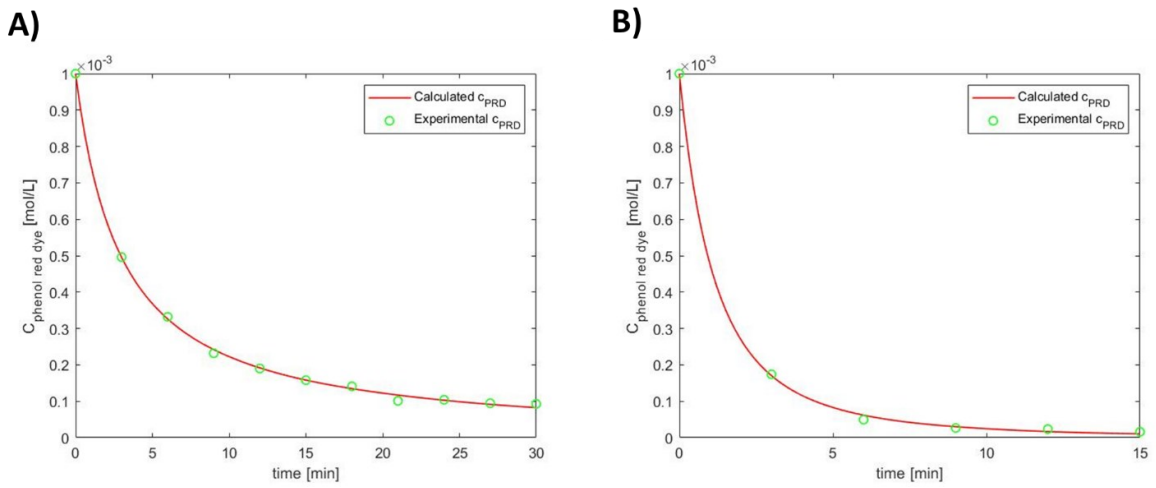

Figure 4.12 - Predictions vs experimental data along the reaction time of PRD reduction with a non-elementary reaction at A) 30°C and B) 40°C

It can be observed that the fitting with α is better with respect to the use of a first-order kinetics. All experimental data are well described by the kinetic model using α, both at 30°C and at 40°C. This result is confirmed by the parity plot with the bands of relative errors of ±10% (Figure 4.13). It can be observed that comparing the parity plot at 30°C of a first-order kinetic and a non-elementary reaction with $\alpha > 1$, the situation is completely different because in the case of $\alpha = 1$ all the data are outside the bands, while with $\alpha > 1$, all the data are inside. The best choice is to use alpha different from one, since the predictions describe better the experimental measurements.

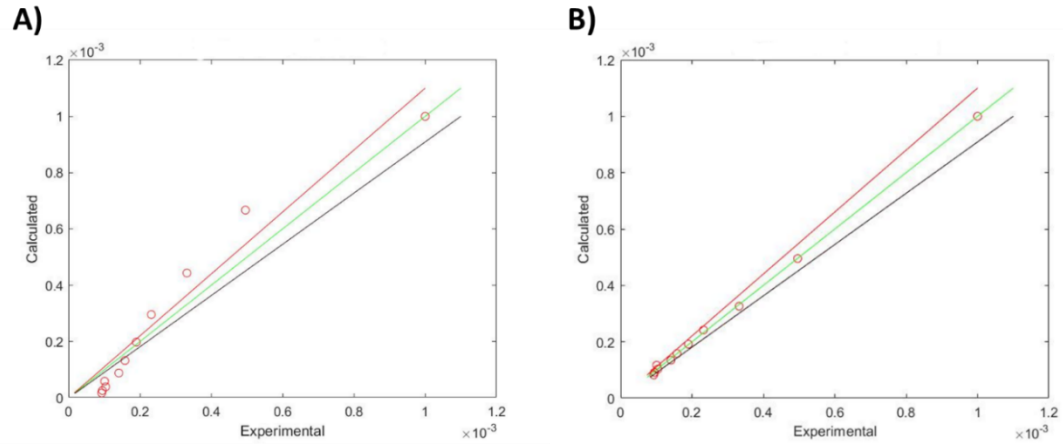

Figure 4.13 - Predictions vs experimental value of PRD reduction at 30°C with bands of relative errors of ±10% of kinetic study assuming A) a first-order reaction and B) a non-elementary reaction

From the results, two different values of α were obtained at the two different temperatures, but temperature can affect only kinetic constants k, whereas α is independent from temperature. Consequently, $\alpha = 1.95$ was chosen and corresponding results are reported in Figure 4.14 and Table 4.6, starting from an initial value of k equal to 0.8.

Table 4.6 *- Final values of kinetic constant obtained through the kinetic study applied to experimental measurement at different temperature for phenol red reduction assuming a non-elementary reaction*

	k [$mol^{-0.95} L^{0.95} \cdot s^{-1}$]	**α [-]**
30°C	236.4	1.95
40°C	1526.3	1.95

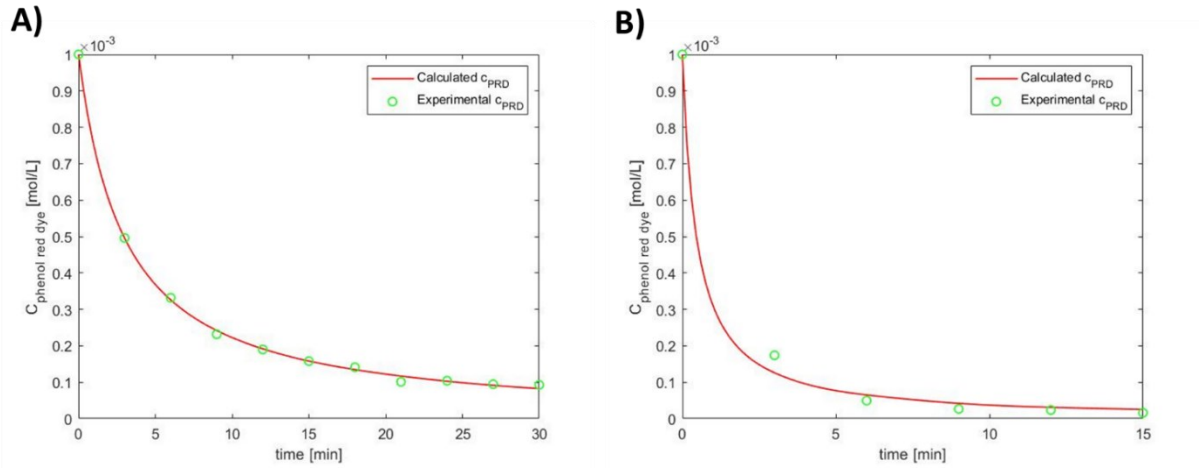

Figure 4.14 - Experimental concentration vs calculated concentration over reaction time of PRD reduction assuming a non-elementary reaction with α = 1.95 for experimental measurements at A) 30°C and B) 40°C

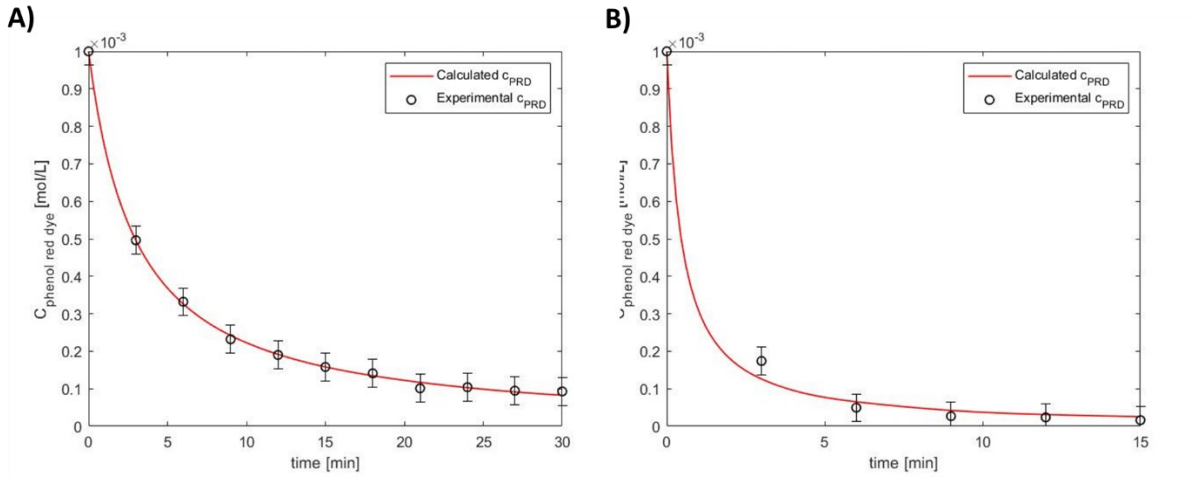

Figure 4.15 - Experimental concentration vs calculated concentration over reaction time with error bars of PRD reduction assuming a non-elementary reaction with α = 1.95 at A) 30°C and B) 40°C

As in the case of PNA, errors bars can be added to Figure 4.14 to confirm the effectiveness of the kinetic model used for PRD reduction. Using the calculation of the standard deviations performed in §3.2.2.8, errors bars with σ half-width were used. It is correct to assume that the kinetic model accurately reproduces the kinetics of the reaction under study, because the calculated concentration curve enters all bands, except for the 3-minute value for data at 40 ºC (Figure 4.15).

4.3.3 Calculation of activation energy and pre-exponential factor for PRD reduction

Pre-exponential factor and activation energy were obtained with Arrhenius law (Equation 4.19). The logarithmic form (Equation 4.20) was used, and with a linear regression on MATLAB the two desired values were computed. Figure 4.16 shows the polynomial curve that fits the experimental points $(\ln k, 1/T)$. It was obtained $E_a = 147060\ J\ mol^{-1}$ and $A = 5.33 \cdot 10^{27} s^{-1} mol^{-0.95}\ L^{0.95}$.

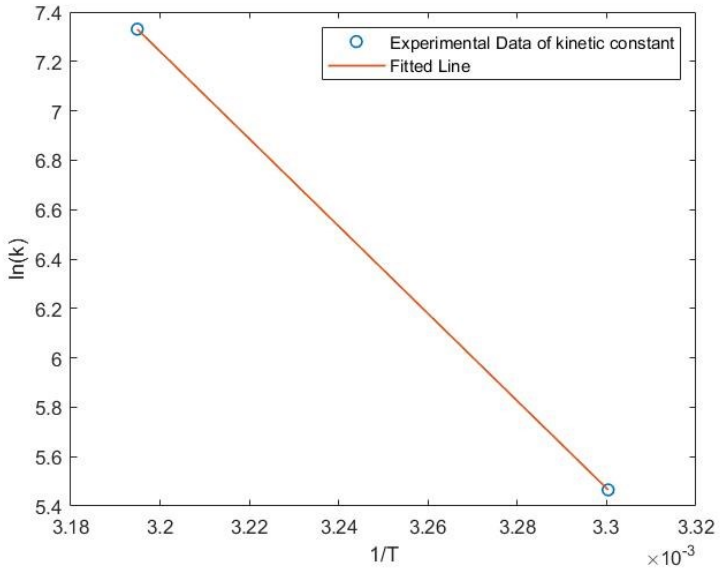

Figure 4.16 - Experimental values of k vs fitted line obtained with linear regression employing Arrhenius equation

A model with first order kinetics was used at the beginning for the kinetic study that was conducted for both reactions. After that, the order of the kinetics was changed because it was thought that a model with an alpha different from one would suit the data better. The results show that this theory is correct. Therefore, it is possible to conclude that for this kind of system,

a kinetic model that is relatively simple but with an alpha value different from 1, specifically $\alpha = 0.75$ for PNA and $\alpha = 1.95$ for PRD, can be used.

Conclusion

The aim of this work was to find an efficient and effective method for the removal of organic dyes from wastewater, and particularly to investigate the performances of the synthesized chitosan supported silver nanoparticles catalysts (Ag/CH) in the reduction of the organic compounds used in industries as dyes. Two organic compounds were tested, namely p-nitroaniline (PNA) and phenol red dye (PRD).

Silver nanoparticles supported on chitosan was synthesized and then analyzed with different techniques for the evaluation of the molecular structure (XRD) and the morphology (SEM) of the catalyst, the amount of silver nanoparticles (ICP-OES), the presence of organic and inorganic compounds (FT-IR) on the sample. At room temperature, PNA and PRD aqueous solutions were effectively reduced using the Ag/CH catalyst.

It has been observed that the rate of reaction is influenced by concentration of catalyst, of $NaBH_4$, of dye, and the applied temperature. The rate of degradation of the reactant is zero without Ag/CH in the case of PNA, while PRD degraded even with only $NaBH_4$, but the rate of reaction is higher with both Ag/CH catalyst and $NaBH_4$, compared to non-catalytic approach (only $NaBH_4$). Furthermore, Ag/CH can also decrease the concentration of PRD in the absence of $NaBH_4$ in the solution, possibly due to adsorption process. In the case of PNA, the catalyst is effective in the reduction processes only, with a hydrogen source. The catalyst is recycled five times in both cases, and it showed constant catalytic activities, meaning that it can be reused several times. Ag/CH with different % Ag is efficient, even if the amount of silver on the chitosan support is very low. According to kinetic studies, a first order kinetics for both processes is not sufficient to adequately represent how the experimental concentrations change over time. Instead, a kinetic model containing an adaptive partial reaction order parameter is needed. Results demonstrated that Ag/CH can be considered as an active and recyclable heterogenous catalyst for the reduction of PNA and PRD. Considering the low cost and wide availability of Ag metal precursor as well as bio-based support material, the described approach can also be found to be economically convenient.

Bibliography

Ali, H. (2010). Biodegradation of synthetic dyes—a review. *Water, Air, & Soil Pollution*, **213**, 251-273.

Anbu Anjugam Vandarkuzhali, S., Viswanathan, B., Pachamuthu, M. P., & Chandra Kishore, S. (2020). Fine copper nanoparticles on amine functionalized SBA-15 as an effective catalyst for mannich reaction and dye reduction. *Journal of Inorganic and Organometallic Polymers and Materials*, **30**(2), 359-368.

Akpan, U. G., & Hameed, B. H. (2009). Parameters affecting the photocatalytic degradation of dyes using TiO2-based photocatalysts: a review. *Journal of hazardous materials*, **170**(2-3), 520-529.

Anjaneyulu, Y., Sreedhara Chary, N., & Samuel Suman Raj, D. (2005). Decolourization of industrial effluents–available methods and emerging technologies–a review. *Reviews in Environmental Science and Bio/Technology*, **4**, 245-273.

Asiri, A. M., Al-Amoudi, M. S., Al-Talhi, T. A., & Al-Talhi, A. D. (2011). Photodegradation of Rhodamine 6G and phenol red by nanosized TiO2 under solar irradiation. *Journal of Saudi Chemical Society*, **15**(2), 121-128.

Chauhan, S. S., Jasra, R. V., & Sharma, A. L. (2012). Phenol red dye functionalized nanostructured silica films as optical filters and pH sensors. *Industrial & engineering chemistry research*, **51**(31), 10381-10389.

Chung, K. T., Fulk, G. E., & Andrews, A. W. (1981). Mutagenicity testing of some commonly used dyes. *Applied and Environmental Microbiology*, **42**(4), 641-648.

Edison, T. N. J. I., Sethuraman, M. G., & Lee, Y. R. (2016). NaBH 4 reduction of ortho and para-nitroaniline catalyzed by silver nanoparticles synthesized using Tamarindus indica seed coat extract. *Research on Chemical Intermediates*, **42**, 713-724.

El-Hout, S. I., El-Sheikh, S. M., Gaber, A., Shawky, A., & Ahmed, A. I. (2020). Highly efficient sunlight-driven photocatalytic degradation of malachite green dye over reduced graphene oxide-supported CuS nanoparticles. *Journal of Alloys and Compounds*, **849**, 156573.

Ermrich, M., & Opper, D. (2013). XRD for the analyst. Getting acquainted with the principles. Second. Panalytical.

Fernández, C., Larrechi, M. S., & Callao, M. P. (2010). An analytical overview of processes for removing organic dyes from wastewater effluents. *TrAC Trends in Analytical Chemistry*, **29**(10), 1202-1211.

Frick, J. M., Ambrosi, A., Pollo, L. D., & Tessaro, I. C. (2018). Influence of glutaraldehyde crosslinking and alkaline post-treatment on the properties of chitosan-based films. *Journal of Polymers and the Environment*, **26**, 2748-2757.

Hamed, I., Özogul, F., & Regenstein, J. M. (2016). Industrial applications of crustacean by-products (chitin, chitosan, and chitooligosaccharides): A review. *Trends in food science & technology*, **48**, 40-50.

Hamzavi, S. F. F., Jamili, S., Yousefzadi, M., Moradi, A. M., & Biuki, N. A. (2019). Silver nanoparticles supported on chitosan as a green and robust heterogeneous catalyst for direct synthesis of nitrogen heterocyclic compounds under green conditions. *Bulletin of Chemical Reaction Engineering & Catalysis*, **14**(1), 51-59.

He, K., Chen, G., Zeng, G., Chen, A., Huang, Z., Shi, J., ... & Hu, L. (2018). Three-dimensional graphene supported catalysts for organic dyes degradation. *Applied Catalysis B: Environmental*, **228**, 19-28.

Held, P. (2018). Using phenol red to assess pH in tissue culture media. *BioTek Appl. Note1*, 1-7.

Islam, M. T., Saenz-Arana, R., Wang, H., Bernal, R., & Noveron, J. C. (2018). Green synthesis of gold, silver, platinum, and palladium nanoparticles reduced and stabilized by sodium rhodizonate and their catalytic reduction of 4-nitrophenol and methyl orange. *New Journal of Chemistry*, **42**(8), 6472-6478.

Jiménez-Gómez, C. P., & Cecilia, J. A. (2020). Chitosan: a natural biopolymer with a wide and varied range of applications. *Molecules*, **25**(17), 3981.

Kaloti, M., & Kumar, A. (2018). Sustainable Catalytic Activity of Ag-Coated Chitosan-Capped γ-Fe2O3 Superparamagnetic Binary Nanohybrids (Ag-γ-Fe2O3@ CS) for the Reduction of Environmentally Hazardous Dyes A Kinetic Study of the Operating Mechanism Analyzing Methyl Orange Reduction. *ACS omega*, **3**(2), 1529-1545.

Khan, M. S. J., Khan, S. B., Kamal, T., & Asiri, A. M. (2020). Catalytic application of silver nanoparticles in chitosan hydrogel prepared by a facile method. *Journal of Polymers and the Environment*, **28**, 962-972.

Khataee, A. R., & Kasiri, M. B. (2010). Photocatalytic degradation of organic dyes in the presence of nanostructured titanium dioxide: Influence of the chemical structure of dyes. *Journal of Molecular Catalysis A: Chemical*, **328**(1-2), 8-26.

Kwok, K. C., Koong, L. F., Chen, G., & McKay, G. (2014). Mechanism of arsenic removal using chitosan and nanochitosan. *Journal of colloid and interface science*, **416**, 1-10.

Ma, H., Kong, A., Ji, Y., He, B., Song, Y., & Li, J. (2019). Ultrahigh adsorption capacities for anionic and cationic dyes from wastewater using only chitosan. *Journal of cleaner production*, **214**, 89-94.

Malik, A., & Nath, M. (2020). Synthesis of Ag/ZIF-7 by immobilization of Ag nanoparticles onto ZIF-7 microcrystals: A heterogeneous catalyst for the reduction of nitroaromatic compounds and organic dyes. *Journal of Environmental Chemical Engineering*, **8**(6), 104547.

MeenaKumari, M., & Philip, D. (2015). Degradation of environment pollutant dyes using phytosynthesized metal nanocatalysts. *Spectrochimica Acta Part A: Molecular and Biomolecular Spectroscopy*, **135**, 632-638.

Mittal, A., Kaur, D., Malviya, A., Mittal, J., & Gupta, V. K. (2009). Adsorption studies on the removal of coloring agent phenol red from wastewater using waste materials as adsorbents. *Journal of colloid and interface science*, **337**(2), 345-354.

Naseem, K., Farooqi, Z. H., Begum, R., & Irfan, A. (2018). Removal of Congo red dye from aqueous medium by its catalytic reduction using sodium borohydride in the presence of various inorganic nano-catalysts: a review. *Journal of cleaner production*, **187**, 296-307.

Picollo, M., Aceto, M., & Vitorino, T. (2018). UV-Vis spectroscopy. *Physical sciences reviews*, **4**(4), 20180008.

Ramírez, M. A., Rodríguez, A. T., Alfonso, L., & Peniche, C. (2010). Chitin and its derivatives as biopolymers with potential agricultural applications. *Biotecnología Aplicada*, **27**(4), 270-276.

Saini, R. D. (2017). Textile organic dyes: polluting effects and elimination methods from textile waste water. *Int J Chem Eng Res*, **9**(1), 121-136.

Sargin, I. (2019). Efficiency of Ag (0)@ chitosan gel beads in catalytic reduction of nitroaromatic compounds by sodium borohydride. *International journal of biological macromolecules*, **137**, 576-582.

Sencadas, V., Correia, D. M., Ribeiro, C., Moreira, S., Botelho, G., Ribelles, J. G., & Lanceros-Méndez, S. (2012). Physical-chemical properties of cross-linked chitosan electrospun fiber mats. *Polymer Testing*, **31**(8), 1062-1069.

Sriram, N., Reetha, D., & Saranraj, P. (2013). Biological degradation of reactive dyes by using bacteria isolated from dye effluent contaminated soil. *Middle East J Sci Res*, **17**(12), 1695-1700.

Sun, J. H., Sun, S. P., Fan, M. H., Guo, H. Q., Qiao, L. P., & Sun, R. X. (2007). A kinetic study on the degradation of p-nitroaniline by Fenton oxidation process. *Journal of hazardous materials*, **148**(1-2), 172-177.

Tan, T. K., Khiew, P. S., Chiu, W. S., Radiman, S., Abd-Shukor, R., Huang, N. M., & Lim, H. N. (2011). Photodegradation of phenol red in the presence of ZnO nanoparticles. *International Journal of Materials and Metallurgical Engineering*, **5**(7), 627-632.

Tehrani-Bagha, A. R., Mahmoodi, N. M., & Menger, F. M. (2010). Degradation of a persistent

organic dye from colored textile wastewater by ozonation. *Desalination*, **260**(1-3), 34-38.

Varjani, S., Rakholiya, P., Ng, H. Y., You, S., & Teixeira, J. A. (2020). Microbial degradation of dyes: an overview. *Bioresource Technology*, **314**, 123728.

Wahab, H. S., & Hussain, A. A. (2016). Photocatalytic oxidation of phenol red onto nanocrystalline TiO2 particles. *Journal of Nanostructure in Chemistry*, **6**(3), 261-274.

Wang, S. G., Sun, X. F., Liu, X. W., Gong, W. X., Gao, B. Y., & Bao, N. (2008). Chitosan hydrogel beads for fulvic acid adsorption: Behaviors and mechanisms. *Chemical Engineering Journal,* **142**(3), 239-247.

Wegrzynowska-Drzymalska, K., Grebicka, P., Mlynarczyk, D. T., Chelminiak-Dudkiewicz, D., Kaczmarek, H., Goslinski, T., & Ziegler-Borowska, M. (2020). Crosslinking of chitosan with dialdehyde chitosan as a new approach for biomedical applications. *Materials*, **13**(15), 3413.

Zaharia, C., Suteu, D., Muresan, A., Muresan, R., & Popescu, A. (2009). Textile wastewater treatment by homogenous oxidation with hydrogen peroxide. *Environmental Engineering and Management Journal*, **8**(6), 1359-1369.

Zheng, Y., & Wang, A. (2012). Ag nanoparticle-entrapped hydrogel as promising material for catalytic reduction of organic dyes. *Journal of Materials Chemistry*, **22**(32), 16552-16559.

https://pubchem.ncbi.nlm.nih.gov/compound/Phenol-red (last access 06/03/2023)

https://terpconnect.umd.edu/~choi/MSDS/Sigma-Aldrich/PHENOL%20RED.pdf (last access 06/03/2023)

Acknowledgments

First of all, I would like to thank prof. Paolo Canu for giving me the chance to have an experience abroad and for assisting me with my thesis work. I also want to thank prof. Jyri-Pekka Mikkola for including me in the group, making me feel at home and having assigned me a truly interesting work. A special thanks to Dr. Santosh Govind Khokarale for welcoming me on the first day I arrived in Umea, meticulously following me throughout my stay, and for his ongoing helpful advice. I also want to thank Minh Van Dinh for his kindness and continuous availability to assist me in the lab when I needed it. Last but not least, I want to express my gratitude to the other lab staff members who helped me with my project even though they were not directly involved.